A review of the gas and liquid phase interactions in low-temperature plasma jets used for biomedical applications

Youssef Morabit, Mohammad Hasan, Richard Whalley, Eric Robert, Martina Modic, James Walsh

Eur. Phys. J. D
https://doi.org/10.1140/epjd/s10053-020-00004-4

Topical Review

A review of the gas and liquid phase interactions in low-temperature plasma jets used for biomedical applications

Youssef Morabit[1], Mohammad I. Hasan[1], Richard D. Whalley[2], Eric Robert[3], Martina Modic[4], and James L. Walsh[1,a]

[1] Centre for Plasma Microbiology, University of Liverpool, Brownlow Hill Liverpool L69 3GJ, UK
[2] School of Mechanical and Systems Engineering, Newcastle University, Newcastle NE1 7RU, UK
[3] GREMI UMR 7344 CNRS/Université d'Orléans, 45067 Orléans, France
[4] Laboratory for Gaseous Electronics, Jožef Stefan Institute, 1000 Ljubljana, Slovenia

Received 1 April 2020 / Accepted 3 November 2020

Abstract. Atmospheric pressure plasma jets generated using noble gases have been the focus of intense investigation for over 2 decades due to their unique physicochemical properties and their suitability for treating living tissues to elicit a controlled biological response. Such devices enable the generation of a non-equilibrium plasma to be spatially separated from its downstream point of application, simultaneously providing inherent safety, stability and reactivity. Underpinning key plasma mediated biological applications are the reactive oxygen and nitrogen species (RONS) created when molecular gases interact with the noble gas plasma, yielding a complex yet highly reactive chemical mixture. The interplay between the plasma physics, fluid dynamics and plasma chemistry ultimately dictates the chemical composition of the RONS arriving at a biological target. This contribution reviews recent developments in understanding of the interplay between the flowing plasma, the quiescent background and a biological target to promote the development of future plasma medical therapies.

1 Introduction

Atmospheric pressure plasma jets (APPJ's) are the focus of an intense international research effort due to their unique chemical and physical characteristics. A defining aspect of the plasma jet is the interplay between the plasma physics, plasma chemistry and fluid dynamics, which ultimately dictate application efficacy. Plasma jets can be constructed using a wide variety of electrode configurations and powered using a plethora of high voltage power sources (ranging from DC to GHz). A vast array of different gases have been investigated, ranging from noble gases such as helium and argon through to complex gas mixtures such as humid air. In the context of biomedical and healthcare-related applications, perhaps the most common plasma jet configuration is based on the dielectric barrier discharge (DBD) operating in a noble gas; it allows for the generation of a stable stream of plasma downstream of the high-voltage electrodes with minimal risk of arcing [1]. Given the widespread use of the DBD jet configuration for healthcare-related application, it is chosen as the primary focus of this review.

One of the first applications of a DBD jet created at atmospheric pressure was to inactivate bacteria, as reported by Laroussi and colleagues [2]. In this study a pulsed voltage was applied at kHz frequency to ignite a discharge in flowing helium gas which emerged from the electrodes and impinged on a bacterial target. Since the pioneering early works, a large number of studies have explored the physics and chemistry of the plasma plume as well as the effects of plasma exposure on many different biological targets. It was quickly discovered that spatial separation between the region of plasma generation and reactive species creation makes the plasma jet configuration unique, facilitating a stable source of both short-lived and long-lived reactive oxygen and nitrogen species (RONS) under ambient conditions [3].

Noble gas plasmas are expected to have little chemical reactivity; however, impurities found within the feed gas (e.g. H_2O, O_2 and N_2) can give rise to a variety of RONS. Furthermore, beyond the jet capillary the discharge is free to interact with the quiescent background gas (typically humid air), resulting in the creation of an abundance of reactive chemical species. While such interactions act to increase the reactivity of the plasma, the unpredictable composition of the ambient background has the potential to alter the physicochemical processes at play reducing the repeatability of any downstream treatment. In order to understand and ultimately control the composition of RONS within the plasma, considerably more insight is required into

[a] e-mail: jlwalsh@liverpool.ac.uk (corresponding author)

Published online: 21 January 2021

the complex interactions occurring beyond the capillary. While the physics of the plasma jet are now well understood, the impact of the quiescent background on the physicochemical processes at play have been mostly overlooked due to the complexity of the interaction. Several studies have probed the interaction via qualitative methods, such as Schlieren imaging [4–8], observing that plasma generation has a marked impact of the fluid dynamics of the system. Particle image velocimetry has been used to quantitatively study a free submerged axisymmetric plasma jet and characterise the plasma-induced turbulence [8,9]. Both qualitative and quantitative methods confirm that the presence of a discharge generated at kHz frequencies within a flowing gas results in perturbation of the jet flow and the early onset of turbulence [8,10–12].

In terms of application potential, DBD based plasma jets have been widely investigated for use in high-value materials processing and more recently in the biomedical area. Many studies on the use of plasma jets to inactive bacteria, fungi and viruses commonly found in the agricultural [13–15], and healthcare sectors [16–18], have shown promising results. In a parallel development, the use of DBD jets in the field of 'plasma medicine' has garnered much interest, with studies on the ability of the plasma jet to stimulate wound healing [19,20], kill cancer cells [21,22], and modulate immune response [23,24], both in vivo [25,26], and in clinical trials [27]. This contribution summarises the recent developments in the field of DBD plasma jets with a focus on the interactions occurring beyond the jet capillary. The link between the discharge physics, plasma chemistry, background gas and sample composition is considered and the latest findings in the field of microbial inactivation and wound healing are considered.

The remainder of this article is divided into five sections, the first of which provides a summary of the major plasma jet configurations used in the field, and a discussion of the physical mechanisms giving rise to the fast ionisation wave or 'plasma bullet' phenomena typically observed. The second section explores the interaction of the plasma jet with the quiescent background, with a specific focus on a helium free jet impinging in ambient air. The third section explores the physicochemical processes at play when plasma interacts with moist and liquid-like samples, as these are typically found in biological applications. Section four explores recent biomedical application of plasma jets, with a specific focus on applications relating to microbial decontamination and wound healing. Finally, an outlook on the future perspectives of plasma jet use in emerging biomedical applications is presented.

2 Plasma jet devices and principal of operation

2.1 Typical jet configurations

A key advantage of the APPJ configuration is its ability to generate a stable and controllable column of plasma extending beyond the confines of the electrodes and into the surrounding environment. Of all the possible APPJ configurations, the DBD jet configuration is perhaps the most widely used and generally consists of a flowing noble gas through a dielectric capillary, impinging into the ambient air. An electrode system in or around the capillary is used to apply a time-varying voltage of sufficient magnitude to initiate breakdown within the capillary, thus generating a plasma column extending from the capillary into ambient air. Accordingly, the choice of feed gas plays a major role in determining the composition of reactive species. For example, when helium with an oxygen admixture is used as the feed gas, the generated reactive oxygen species (e.g. O, $^1O_2$, O_3) are well suited to microbial inactivation applications [28–32].

An additional factor influencing the characteristics of an APPJ is the choice of electrode configuration. Figure 1 shows a selection of the most common electrode configurations used in APPJ discharges. Configurations shown in Fig. 1a–c employ a coaxial electrode within the dielectric capillary to generate the discharge [4,30,33–41], an advantage of this configuration is the reduced breakdown voltage; however, a drawback of this configuration is the lack of a dielectric between the driven electrode and a downstream sample, which makes the system more liable to arcing. Configurations (d) and (e) employ ring electrodes positioned on the outside of the capillary, acting to enhance electrical safety at the expense of an increased breakdown voltage [8,42–46]. The chosen electrode configuration can also affect the shape of the plasma plume beyond the capillary, thus influencing the generation and the transport of reactive species [36,47]. In all cases, when a single electrode is employed, capacitive coupling to ground provides a return path for current flow. In most cases, the downstream sample acts as the ground electrode and consequently the plasma properties can be strongly influenced by the sample composition.

Specific applications require custom variations of the typical APPJ discharge configuration; for example, APPJs developed for applications in endoscopy require meter long flexible capillaries able to produce a stable column of plasma [48–56]. For applications where power consumption is a concern or additional safety is required, an APPJ with a dielectric-covered pin electrode can generate a discharge with similar properties to those with an uncovered pin electrode configuration at much lower power [57]. Another design consideration is user safety, which is especially important when the intended application is a medical treatment. The kINPen MED was the first APPJ accredited as a medical device with a certified electrical safety, this plasma

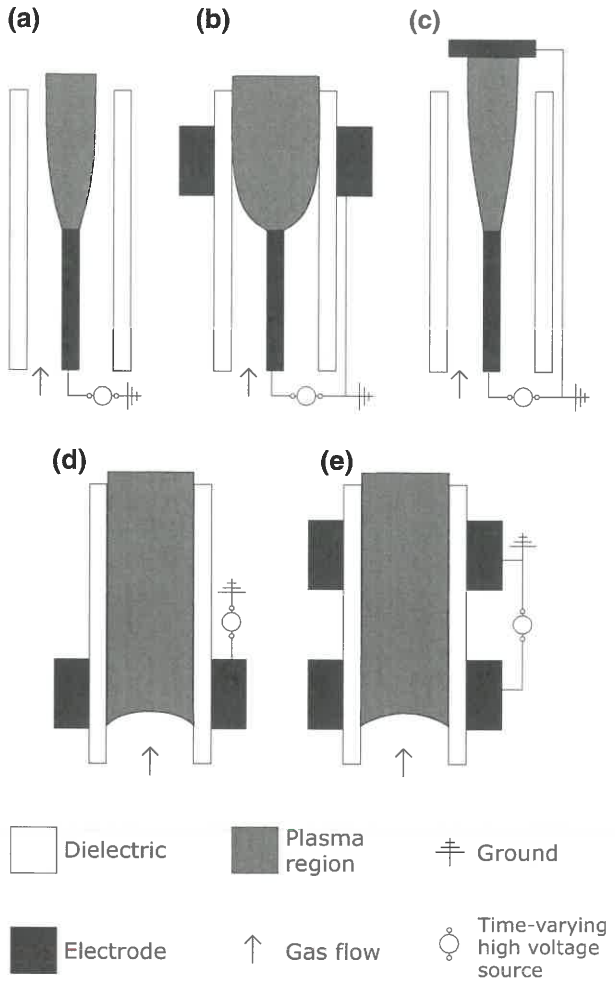

Fig. 1 Cross sectional views of commonly used low-temperature plasma jet configurations: **a** Powered pin electrode with floating ground, **b** powered pin electrode with ground electrode wrapped around dielectric capillary, **c** powered pin electrode with grounded downstream target, **d** single powered electrode wrapped around dielectric capillary, and **e** powered and ground electrodes wrapped around dielectric capillary

source serves as a standard towards biomedical studies [58].

A downside of APPJs is the relatively small area of treatment covered by the plasma, which is typically on the order of few mm^2 [59]. It represents a challenge to the scalability of the discharge and thus limits its potential for large scale applications. In order to overcome this problem, multiple APPJs can be combined into arrays to maintain the advantages of a single APPJ while simultaneously increasing the treatment area. In some studies, each APPJ in the array has an individual gas feed [60–63], while in others all the jets share a single gas feed [60–62,64–66], both expand the plasma-target area of contact. A drawback of arraying multiple APPJs is gas consumption, which can quickly become prohibitively expensive when noble gases are used. Furthermore, due to the electrical characteristics of the plasma column emerging from each individual capillary in an APPJ array, the interaction between discharges is inevitable. Several studies have shown that individual plasma columns within an array can either repel or attract each other depending on their characteristics acting to reduce downstream treatment uniformity of a sample [60,67].

2.2 Fast moving ionisation waves

When APPJs are in operation, a continuous luminous plasma plume can be seen by the naked eye; however, such observations do not show the true nature of the discharge. Using short-exposure imaging techniques the plasma plume has been revealed to consist of a sequence of Ionization Waves (IW) propagating at high speeds in the order of 10^5—10^8 $cm\,s^{-1}$ [68–71]. IWs are present in dielectric barrier discharges, where ionisation occurs in a small volume that changes position over time, this volume is characterised by a strong electric field, which energises electrons and leads to dissociation and ionisation of the feed gas by electron impact. IWs, also known as plasma bullets, are ignited near the driven electrode when the externally applied electric field exceeds the breakdown voltage in the feed gas [29,71–77], as they propagate they create a conductive channel connecting them to the powered electrode [78,79]. The electric field supports the propagation of the IW; thus, the voltage pulse duration is a key factor on the propagation length. As IW's continue to propagate, the finite conductivity of the plasma channel weakens the electric field, until they arrive at a position where the direct ionisation rate drops as a result of changing gas composition and the weakened electric field, which typically occurs at a distance of a few cm's downstream of the capillary orifice [29]. Inside the capillary, the IW expands radially and propagates along the capillary inner wall, in what is known as a "wall-hugging" mode [80]. Beyond the confines of the capillary, 'doughnut-shaped' structure of the IW evolves in to a more 'homogenous' structure as it propagates downstream, which has been attributed to the diffusion of air into the feed gas flow [71]. The IW propagation mechanism can differ when a more complex electrode configuration is adopted, propagation in a long flexible capillary or a glass loop showed the IW tendency to hug one wall due to curvature [56,81]. Moreover, in the generation of a plasma array, a primary propagating IW ignites secondary IWs originating from holes located along the tube [67].

The electric field at the tip of the IW has a significant influence on its characteristics. For instance, the speed of the IW is directly correlated with the strength of the electric field at its tip; a strong electric field increases the velocity of the IW [82]. The electric field of the IWs decreases as they move towards the exit of the capillary, which is explained by electric potential screening as a result of surface charging of the inner walls of the capillary [83,84]. The electric field then increases when the IWs exit the capillary, this effect is attributed to

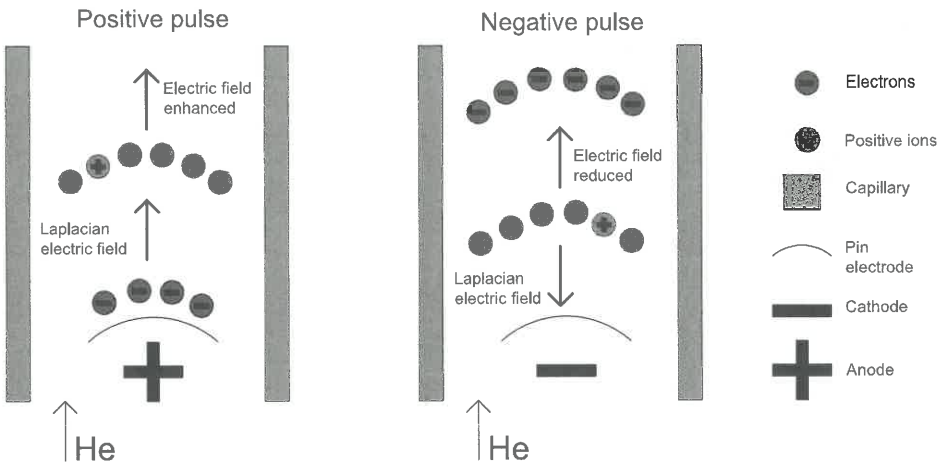

Fig. 2 The electric field distribution with positive and negative pulses in a plasma jet

the contraction of the IWs as they are moving away from the capillary, which strengthens the electric field by focusing the charge density of the IWs into a smaller volume [85], leading to an increase in the IWs propagation speed [82,86,87].

The polarity of the applied voltage driving the discharge influences the strength of the total electric field at the front of the IW. The total electric field governing the IW propagation results from the combination of a space charge induced electric field with the Laplacian electric field associated with the electrode polarization. Figure 2 shows the influence of the polarity on the total electric field for a pulse driven APPJ [88]. For positive polarity cases, the total electric field increases as a result of the addition of the external electric field and the space charge induced field [88]. In the case of a negative polarity, the total electric field is weakened as the external electric field and the space charge induced field to subtract from each other, as highlighted in Fig. 2 [88]. In most cases, the space charge electric field has a higher transient amplitude than the Laplacian electric field. Moreover, standard configurations with the input voltage on the order of few kVs generates an electric field in the tens of kV cm^{-1} [82,89]. Bourdon et al. measured the peak value of the electric field along the plasma plume generated by a pulse driven helium APPJ at 45 kV cm^{-1}, in agreement with computational modelling prediction [84]. The generation of strong external electric fields in a plasma jet has increased interest in the use of such systems to manipulate cellular membranes, leading to poration or apoptosis. Electric field strengths in the range of 10–100 kV cm^{-1} influences the field-dependent relative permittivity of the membrane [90]. A maximum electric field value up to 170 kV cm^{-1} in the sheath at the surface of a water layer was estimated with computational modelling by Norberg et al. [91]. While Begum et al. experimentally measured, with optical emission spectroscopy, the maximum local electric field of 95 kV cm^{-1} at 13 mm from the tube exit for a nanosecond pulse plasma pencil (4–8 kV, 500–800 ns, 4 kHz) [87].

The application of an external electric field can alter the ionisation wave's propagation characteristics. For example, the application of an external field perpendicularly to the propagation direction of the IW causes its propagation path to bend in the opposite direction of the external field [42,92]. The propagation velocity of the IW can be decreased along the axis of propagation by placing a positively biased downstream ring or plate electrode. The opposite effect can be induced by negatively biasing the downstream electrodes [42,93]. Simulations show that a negatively biased downstream electrode increases the electric field of the IW, thus, increasing the propagation speed, whereas a positively biased downstream electrode reduces the electric field of the IW and causes a decrease in the propagation speed [42]. Wang et al. observed the IW velocity decays at a faster rate as it travelled downstream when the pulse frequency increased from 1 to 3 kHz on a pulse driven APPJ using a powered pin electrode in a quartz capillary, although the peak velocity was unchanged [34]. They explained this effect by the increased number of charged species in the bullet head and faster recombination speed at higher pulse frequency. The increase of the pulse repetition rate produces an accumulation of charge deposition on the surface of the inner capillary, affecting the plasma column by inducing an electric potential shielding [94]. This results in an observed increase of the propagation velocity of the IW; thus, a lengthier plasma plume [95]. The addition of a dielectric target and the deposition of positive charge on the surface of the target weakens the electric field and encourages the streamer head into a radial propagation towards areas with stronger electric field [96].

The characteristics of the ionisation waves are also dependent on the feed gas, including the feed gas type and flow rate. The feed gas is usually helium or argon, although more exotic noble gasses and gas mixtures have been explored. The choice of feeding gas has a major impact on the physicochemical processes at play. For example, the role played by the Penning ionisation in helium fed APPJs has increased the propagation

speed of an IW, compared to that observed in argon for similar configuration [35,97]. While the flow rate does not directly affect the physical properties of the jet, it influences the mixing of impurities downstream of the capillary and thus is able to impact ionisation and attachment processes altering the charge density and the electric field distribution [85,98].

The strong electric field in the ionisation wave originates from a strong charge imbalance. In cathode directed IWs, positive ions dominate over electrons and negative ions, while in anode directed IWs, negative ions and electrons dominate [99]. The charged species move under the influence of the electric field while colliding with the molecules of the feed gas, leading to a net momentum transfer from the charged species to the feed gas. This momentum transfer appears as an effective force known as the Electrohydrodynamic (EHD) force [100]. The EHD force has three components in terms of the physical mechanism involved, of which the dominant component is the electric field [100]. The impact of EHD forces in an APPJ has been investigated experimentally by Park et al. and computationally by Hasan et al. [69,101]. Park et al. studied a helium APPJ driven by varying length voltage pulses, using a combination of experiments and modelling, they showed that the residual charge after the collapse of IWs also contributed to the EHD force [69].

3 Link between fluid dynamics and APPJ physicochemical properties

A considerable effort has been directed towards identifying the mechanisms that link the dynamics of the propagating plasma to the flow effects observed in the gas channel emerging from the jet orifice. Many studies have demonstrated that the generation of plasma in a flowing noble gas jet leads to an abrupt laminar-turbulent transition of the flow beyond the orifice. Both EHD forces and gas heating have been suggested as possible mechanisms to explain the dramatic change in flow dynamics, with EHD forces being considered as the dominant factor in kHz excited APPJ's. Notably, the predicted impact of these two phenomena to the flow velocity of the jet falls below what would be required to explain the observed reduction on the laminar region of the jet.

The turbulent flow field generated by variable-density jet is characterised by a dimensionless parameter called the Froude number, Fr $(= \mathrm{U_m^2 \rho_j / gD(\rho_a - \rho_j)})$, which is the ratio of the momentum flux to buoyancy flux of the fluid flow. Where, U_m is the jet exit velocity, ρ_j is the density of the noble gas, ρ_a is the density of the ambient fluid, g is the acceleration due to gravity and D is the inner diameter of the capillary. When a helium based APPJ is orientated to generate a turbulent jet flow in the upwards direction, the developing flow field is divided into three distinct regions [102], which are functions of increasing vertical distance away from the jet exit. First, there is a region of pure jet behaviour driven by momentum flux. At the end of the pure jet region, the fluid flow enters into an intermediary region where both the momentum flux and buoyancy flux play equally important roles. Finally, the jet flow is driven by buoyancy forces.

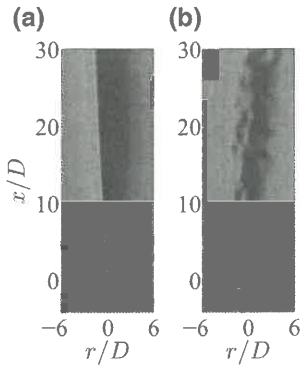

Fig. 3 Schlieren photography of **a** helium jet flow at Re = 135 and helium jet flow at $Re = 135$ with plasma ignited at **b** 16 kV [8]

To date, one of the most extensive pieces of research characterising the developing turbulent flow fields generated by an APPJ was been conducted by Whalley and Walsh [8]. High-speed Schlieren imaging and 2D PIV were used to investigate the developing turbulent flow fields within the pure jet region of helium APPJs. Figure 3 shows instantaneous Schlieren imaging of a helium APPJ flow at a Reynolds number of $Re = U_m D/\nu_j = 135$, where ν_j is the kinematic viscosity of helium. The Reynolds number is a ratio of inertial forces to viscous forces present within the fluid flow and is an essential non-dimensional parameter used to describe the state of the flow (*e.g.* whether the flow is laminar, turbulent or in a state of transition-to-turbulence). Without plasma generation, Fig. 3a, the fluid flow remains laminar. However, the generation of a plasma plume, Fig. 3b, leads to an abrupt transition into a turbulent regime. These types of qualitative observations on plasma-induced turbulent jet flows are well-known within the APPJ community [6,7,43]. Generally, these turbulent flow fields have been observed in APPJ's with Reynolds number ranging from $Re = 135$–840 using both pulsed and sinusoidal excitation with applied voltages from 4 to 30 kV. The frequency of excitation is known to be an important parameter. Within the fluid dynamics communities, frequencies are often represented by a non-dimensional parameter called the Strouhal number, $St = f\theta/U_m$, where f is a characteristic frequency, θ is the momentum thickness of the shear layer at the jet exit, which characterise oscillations within the fluid flow.

The shear layers (i.e. velocity gradients) at the jet exit are highly unstable [103,104]. Small finite perturbations with amplitudes on the order of 10% of the mean jet exit velocity, which contain frequencies with a Strouhal number of $St < 0.04$, can grow exponen-

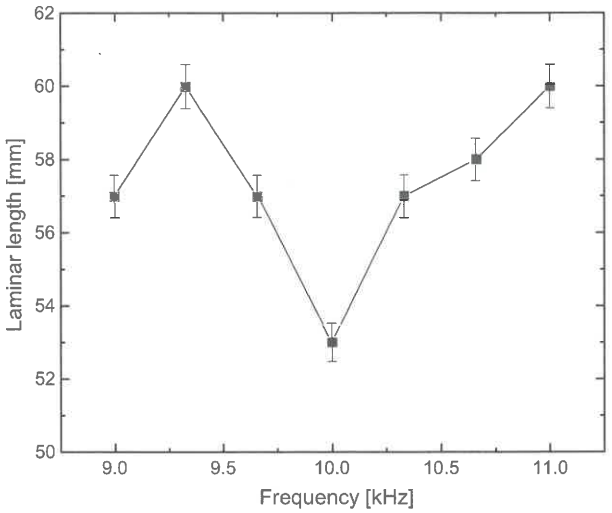

Fig. 4 Laminar region length obtained from ensemble-averaged velocity measurements for a pulse driven plasma jet (1μs pulse width, 6.5 kV amplitude) fed with helium at 3.7 SLM. The repetition frequency varied between 9 and 11 kHz

tially in the unstable shear layers and laminar transition jet flows into turbulent regimes from a Reynolds number as low as $Re \approx 50$ [12,105–107]. Linear stability theory [6,12,29,108–110] and many experimental observations [10] of, albeit, homogeneous (i.e. constant density) axisymmetric jet flows predict that small finite perturbations will amplify the most within the jet shear layers when they have a dominant excitation frequency of $St \approx 0.017$. To put this into context, with volume flow rates of a few standard-litres-per-minute typical for APPJ flows through capillaries which have internal diameters of a few mm's, typical dominant frequencies of 10's of kHz are to be expected, often coinciding with the frequency of plasma excitation.

To demonstrate this, a pulsed plasma jet (1μs pulse width, constant power operation) was used to excite a helium flowing through a quartz capillary at 3.7 SLM. Under such conditions the dominant Strouhal number ($St \approx 0.017$) gives rise to an excitation frequency of approximately 10 kHz. By varying the pulse repetition rate from 9 kHz to 11 kHz the impact of plasma generation on the laminar region length was examined using particle image velocimetry, Fig. 4. The results fitted the prediction from the Strouhal number with a reduction in laminar region length at $f_0 = 10$ kHz. The velocity decay rate is similar along the laminar region for all repetition frequency tested, the most considerable transition-to-turbulence position disparity is observed between the shortest laminar region at 10 kHz and the longest at 11 kHz.

Global instability modes in low-density axisymmetric jets have been found to scale as $fD^2/\nu_j \sim Re(D/\theta)^{1/2}(1+(\rho_j/\rho_a)^{1/2})$, consistent with dominant frequencies on the order of 10's of kHz for APPJ flows [111]. Whalley and Walsh posited that the sudden onset of turbulence generated within an APPJ flow was due to a combination of small-amplitude electro-hydrodynamic body forces and gas heating causing perturbations in the unstable shear layers at the jet exit [8]. These perturbations amplify as they travel downstream causing velocity fluctuations, Reynolds shear stresses and thus the production of turbulence. They estimated with an order-of-magnitude analysis that the combined contribution of these perturbations could increase the mean jet exit velocity by up to 10%. Morabit et al. provided the first quantitative velocity measurements of a plasma jet impinging into ambient air, summarised in Fig. 5 [9]. The ensemble-averaged velocity measurements and normalised centreline velocity decay shows the transition to turbulence induced by the plasma discharge. In the study, the generation of an intense discharge within the jet capillary was found to yield only a relative minor 0.94 m/s increase in flow velocity compared to when the plasma was off, representing a 10% increase, coinciding well with the predictions made in earlier studies [8].

Morabit et al. also used Laser-induced Fluorescence to investigate the influence of fluid dynamic effects, such as shear layer perturbation and turbulence, on the plasma chemistry of the discharge. Figure 6 shows the measured and computed LIF decay time as a function of downstream spatial position for a helium APPJ expanding in ambient air [9]. The LIF decay time is shorter at all spatial positions under both 10- and 14-kV excitation compared to what would be observed under idealized laminar conditions. This result provides experimental evidence supporting the hypothesis that plasma generation increases the entrainment of air within the helium jet at all spatial positions, not just the fully turbulent region. The calculated decay times closely match the measured data points, with both cases showing the agreement.

Furthermore, the study demonstrated that the density of ground state OH at any given downstream position in the jet is strongly influenced by both the discharge characteristics and its interaction with the quiescent background gas. Though it is generally assumed that a higher plasma generation voltage results in enhanced production of OH, Fig. 7 clearly shows that this only holds true close to the jet orifice. With increasing voltage comes increasing entrainment, which ultimately begins to quench the discharge and negatively affects downstream OH production. Counterintuitively, at a position of 16 mm from the jet exit, there is an order of magnitude more OH from a plasma generated using 10-kV compared to one generated using 14-kV excitation. These findings demonstrate that the small-scale shear layer perturbations near the jet orifice act to enhance entrainment of quiescent air, increasing the production of species such as OH, while acting to quench the discharge further downstream.

While many studies have considered the interaction of an APPJ and the quiescent ambient air, this typically does not correspond to a realistic usage scenario when an APPJ is used in a biomedical application, where the plasma not only interacts with the background gas but also impinges on a target substrate.

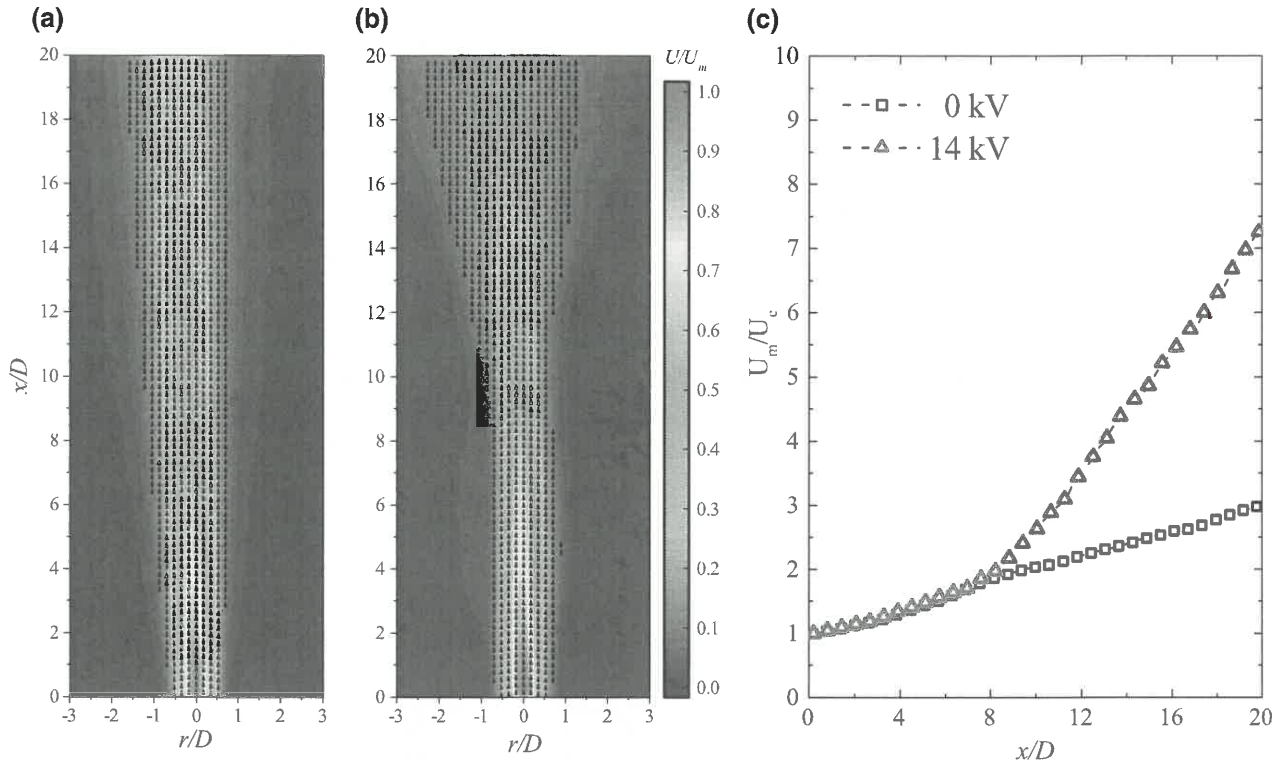

Fig. 5 Ensemble-averaged particle image velocimetry measurements of the plasma jet obtained at applied voltages of **a** 0 kV and **b** 14 kV, **c** shows the reciprocal of the ensemble-averaged centreline velocity (U_c) normalised to the measured exit velocity(U_m) [9]

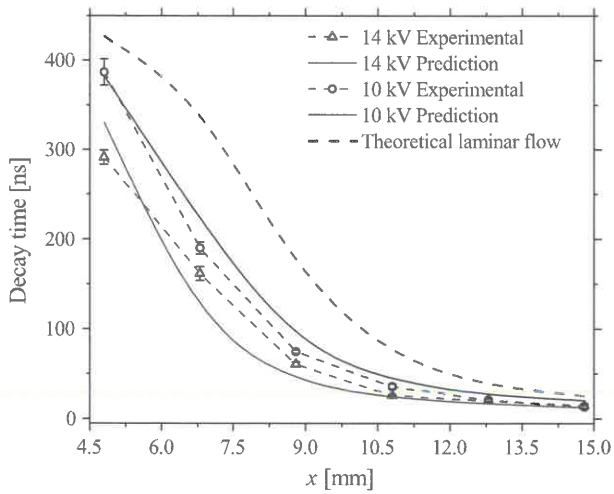

Fig. 6 Comparison between experimental and predicted decay time of the laser-induced fluorescent signal as a function of downstream distance from the atmospheric pressure plasma jet orifice [9]

However, a downward directed noble gas jet bends upward due to the upward buoyancy force overwhelming the diminishing natural inertia of the flow. In the presence of plasma, the natural inertia of the flow is combined with the 'ionic wind', counteracting the buoyancy force and allowing the development of the APPJ downward onto a target [112]. This work [112] reveals the critical role of large and long lifetime negative ions during repetitive operations in the kHz regime, inducing strong modifications in the gas propagation. The cumulative added streamwise momentum transferred to ambient air surrounding molecules resulting from a series of applied voltage pulses induces a gradual built up of a helium channel on tens of millisecond timescale. Although the APPJ can be applied downward, the pulse repetition rate and the nature of the target are crucial factors on the development of the structure of the jet [5,112]. Boselli et al. used high-speed Schlieren imaging to observe a helium plasma jet with and without a target [6]. Their study showed that the fluid dynamics change between the plasma on and off cases; with the presence of instabilities noted in the plasma-on case. The generation of turbulent structures was more visible with a metallic substrate than with a dielectric covered metallic substrate. These observations were attributed to charge deposition on the dielectric surface limiting the current, whereas the conductive substrate behaved like a counter electrode, causing a dramatic shift in the dynamics of the discharge and likely resulting in less perturbation to the jet shear layer.

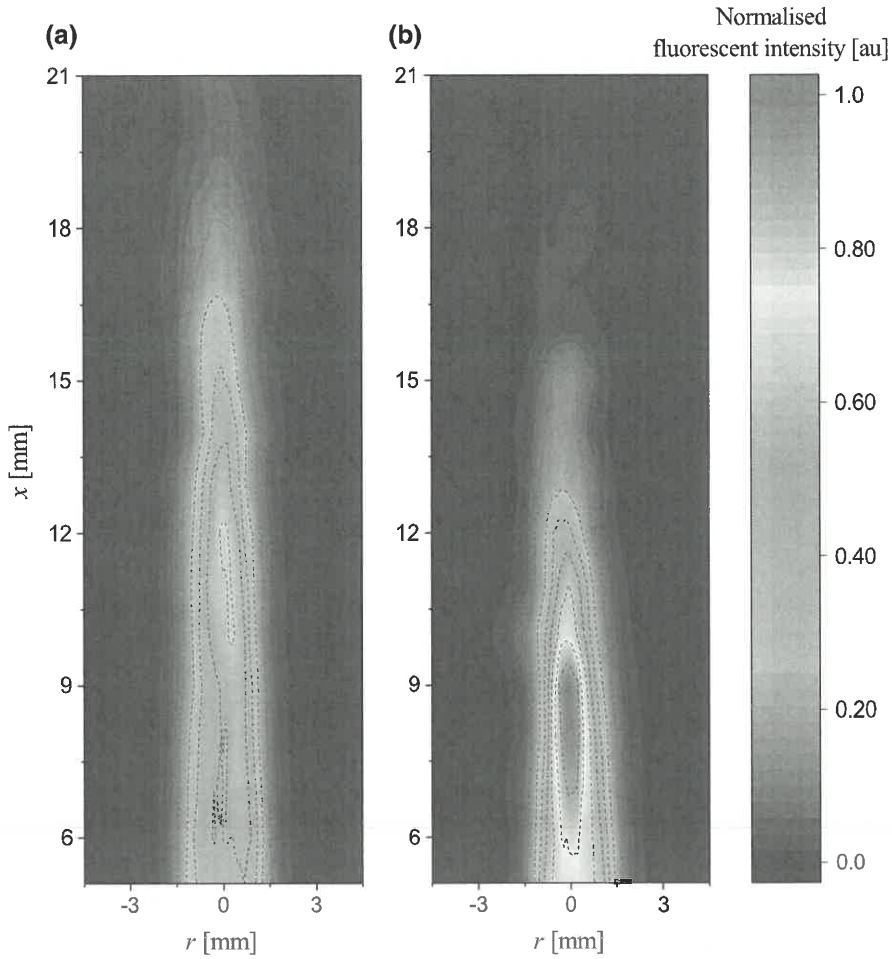

Fig. 7 Composite two-dimensional normalized laser-induced fluorescence intensity of ground state OH for **a** 10 kV and **b** 14 kV applied voltages [9]

4 Liquid and biological target interactions

In biomedical applications, the interaction of an APPJ with a wet or moist sample is almost inevitable; thus, a clear understanding of plasma-liquid interactions is vital for the further development of plasma-based healthcare technologies. The complex interaction between a plasma and a liquid has been widely studied, and a large number of physical and chemical processes have been observed to occur at the plasma-liquid interface.

When treating a liquid sample with an APPJ, the depth of the liquid has a significant impact on the induced chemistry, which is particularly important when a sample is surrounded by a thin liquid layer. Thin liquid films do not allow for convection to occur in the liquid phase, thus the presence of reactive species is due solely to the solubility of the gaseous species. In contrast, thick (or bulk) targets allow for convective transport to develop in the treated media, thus influencing the transport of the reactive species and their chemistry as well [83,113].

When a liquid volume or moisture rich sample is treated with an APPJ, it is inevitable that water vapour from the sample will be entrained within the flowing gas and thus potentially alter the chemistry of the discharge. Several studies have demonstrated that treatment of a liquid target with an APPJ can enhance the production of OH radicals and other species such as HO_2, NO and NO_2 [83,113]. In addition to altering the chemistry in the gas phase, the chemistry of the target itself is also influenced. Understanding this bi-directional coupling between the APPJ chemistry and the target's chemistry is of fundamental importance for biomedical applications.

The APPJ treatment effects on a biological target has been attributed to a combination of reactive species, UV radiation, heating, and electric fields. Of these phenomena, it is the reactive species created at the plasma-liquid interface which are considered to be of primary importance. Verlackt et al. developed a 2D axisymmetric fluid dynamics model to investigate argon APPJ interaction within a buffered aqueous solution [113]. Providing insight on the chemistry in the gas phase, interface and the bulk liquid target.

In the gas phase, the short-lived species O, N, OH, HO_2 and NO_3 participate in the production of long-lived species H_2O_2, O_3, HNO_2 and HNO_3 [113]. At the liquid interface, the gas phase species can dissolve in the interface, and produce long-lived species such as H_2O_2, HNO_2/NO_2^-, $ONOOH/ONOO^-$, O_3 and NO_3^- [113]. The presence of water vapour, whether from the feed gas or due to vaporisation of a liquid target, increases the aqueous H_2O_2 concentration up to a specific limit at which water vapour starts to influence and disrupt the plasma [114,115]. The distance between the jets exit and the liquid target is critical as a short distances limits diffusion of ambient air into the plasma, thus reducing the concentration of precursors important for the production of RONS [116,117]. In contrast, when the distance between the jet and target is considerable, concentrations of shorter-lived RONS can decrease as they react to form more stable species [114,117]. The treatment time also has a significant influence on the aqueous phase chemistry. For instance, a helium APPJ treatment increased the concentration of NO and H_2O_2 in the treated media, the concentration of H_2O_2 being ten times higher than that of NO [116].

The complex chemical nature of plasma-activated liquid presents an exciting research challenge. It is important to consider not only what reactive species are formed as a result of plasma interaction, but how they subsequently react in the liquid phase to produce secondary compounds. For example, Zhou et al., compared the ability of the plasma-activated water and selected chemical agents for the disinfection of *E. coli* bacteria [118]. The results were found to be dependent on the treatment time, with the trend being a stronger effect for longer treatment up to 30 min. Isolated chemical agents such as NO_3^-, NO_2^-, H_2O_2, O_3 and OH showed poor efficacy (< 1 Log reduction), however, combinations such as $NO_2^- + H_2O_2$ and $NO_2^- + NO_3^- + H_2O_2$ had stronger results (up to 4 Log reduction for 30 min treatment). The generation of peroxynitrite from H_2O_2 and NO_2^- was correlated with the observed reductions. Moreover, the mimicked solution containing the chemical agents $NO_2^- + NO_3^- + H_2O_2 + OH + O_3$ did not reach the same level of reduction obtained by plasma-activated water treatment, thus it was concluded that plasma activation of water is more complex and provides greater antimicrobial efficiency than the sum of its expected chemical agents. Besides activating pure water, alternative mediums for plasma activation are under investigation. While these areas are out of the scope of this review, it is worth noting that many exciting developments have been made. Plasma-activated oil has showed promise for the inactivation of both Gram-positive and Gram-negative bacteria as well as accelerating wound healing processes [119,120]. The means by which activated liquids are delivered to the sample is another area which holds great promise, with plasma-activated mist and aerosols both improving the mass transport of reactive chemical species from the plasma phase to the liquid phase, examples includes improved efficacy in areas such microbial disinfection, viral inactivation and food processing [121–125].

While the plasma jet characteristics influence the gas chemistry and therefore indirectly the target chemistry, the nature of the target also influences the plasma jet. Kovacevic et al. measured the electric field profile in a plasma jet plume touching a liquid surface measuring the increase of the electric field strength along the plasma plume until reaching the target. The electric field became stronger along the plasma plume in both free expanding and with a target, although when near the target, a sharp increase of the electric field strength is observed at low helium flow rates [83,85]. The comparison of two gap distances of 7 and 10 mm, showed that the plasma plume in the longest gap reached a stronger electric field value near the liquid surface [83]. The conductivity of the liquid sample does not significantly alter the electric field strength in the IW experimentally (< 10%) [83].

As stated previously, the treatment of liquid volumes differs from the treatment of thin liquid films due to the presence of fluid motion generated by the plasma jet which can affect the generation and transport of species in the liquid bulk [113]. The induced flow in the liquid phase by the APPJ depends on the velocity of the effluent, which is determined by the capillary-to-target distance, jet orifice diameter and the gas flow rate [113]. A helium APPJ impinging on water-based solution was studied using Schlieren imaging and PIV [126], where it was shown that an increase in the normal and shear forces exerted by the jet on a liquid target causes an increase in the liquid flow velocity and circulation size. The presence of fluid motion alters the generation and transport of species, by the generation of vortexes directly affecting the transmission of species from the interface to the liquid bulk [83,113]. Moreover, Verlackt et al. showed that short-lived species do not reach further than the liquid interface, whereas the long-lived species H_2O_2, HNO_2/NO_2^-, NO_3^-, O_3, HO_2/O_2^- and ONOOH/ $ONOO^-$ were predicted in the bulk liquid during the plasma treatment. HNO_2/NO_2^-, HO_2/O_2^- and O_3 reached the bulk liquid through diffusion and convection [113]. Although O_3, HO_2/O_2^- and ONOOH/ $ONOO^-$ were present in the bulk liquid, only H_2O_2, HNO_2/NO_2^- and NO_3^- were expected to remain in the liquid after plasma treatment. While the species are present in the bulk liquid, the spatial prediction of H_2O_2 density showed a clear non-homogenous distribution. Moreover, Brubaker et al. observed that the interaction between the jet and the liquid can provoke a non-homogeneous decrease in temperature and a reduction of pH [126].

Experimental methods for measuring the concentration of chemical species in the liquid are diverse. One of the most common methods is using chemical probes. Despite their low cost and ease of use, chemical probe selectivity is an issue which arises as the probe can potentially react with multiple species [127]. A standard chemical probe is phenol, which offers a simple method to determine the presence of OH radicals, O_3

and NO/NO_2 radicals as they react with it [128]. Optical absorption spectroscopy has also been used to quantify the concentration of reactive species in a liquid target. For instance, the work of Oh et al. where UV–vis spectroscopy and an automated curve fitting routine was used to quantify the changes in H_2O_2, NO_2^-, NO_3^-, and O_2 concentrations [129]. A major advantage of the approach is that it can be used to make measurements both during and after plasma treatment.

In addition to long-lived species, short-lived species can also be measured using chemical probes through spin trapping methods, where organic reagents are used to react with short-lived species converting them into more stable species that can be measured. Elg et al., used this spin trap method to investigate helium plasma jet interaction with liquid, where TEMP solution reacts with $O/O_2/O_3$ and oxidises into TEMPO; thus, providing relative concentrations of multiple species including O, OH, and O_2^- in the liquid phase [127]. In addition, Gorbanev et al. used spin-trapping, EPR spectroscopy and analytical methods to identify the chemical impact of the feed gas by labelling hydrogen or oxygen isotopes [114]. Their results showed that the presence of O_2 in the feed gas is directly linked to the delivery of $O_3/^1O_2/O$ in the liquid sample; while the generation of H_2O_2 occurs mainly within the jet capillary. Moreover, the generation of ·H and ·OH originate from the discharge effluent, with the concentrations of ·OH, and $O_2^{\cdot-}$ radicals in the liquid phase strongly dependent on the composition of feed gas [114].

5 Recent advances in biomedical applications

The use of low-temperature plasma for microbial decontamination has been under intensive investigation for several decades. Menashi patented the process of low-pressure plasma sterilisation in 1968 [130], and it was mostly used as an alternative to conventional sterilisation processes for temperature-sensitive materials in order to inactivate microorganisms while leaving the surface of the material undamaged [130].

Towards the end of the last century, Laroussi et al. showed that atmospheric pressure plasmas could also be efficient for inactivation of bacteria [2,131]. In this early work, a helium discharge was used to expose *Pseudomonas fluorescens* bacteria for different time periods. Comparisons with UV exposure led to the conclusions that plasma could be more efficient and that UV generated by plasma was not the only factor responsible for bacterial inactivation. Although the report was preliminary work to prove the concept, critical questions were raised on the influence of the feeding gas and the plasma configuration. The inactivation mechanism was also unclear, with the complex chemical and biological processes leading to the death of cells remaining unknown. This pioneering work spurred an international effort to research the interaction of plasma with biological systems, a topic which has become an intensive area of research now known as the field 'plasma medicine' [32,132]. During this time a wide range of plasma applications have been developed for decontamination of various microorganisms, cancer treatment, wound healing and dentistry.

Research groups worldwide have designed a wide range of plasma jets for biomedical application with a variety of physical characteristics, such as electrical parameters, working gas, and gas flow. Additionally, a large number of biological protocols, types of organisms or biological system, medium, and cell density have been examined. Consequently, the vast variety of parameters reported make it difficult to directly compare the results reported in the literature. In an attempt to deal with this problem; the European COST Action MP1011 proposed to develop a well-defined and characterised plasma device that could be used for comparison of plasma parameters and also impact on a set of standardised biological tests [133]. Despite enormous effort to establish this plasma-jet based device, a relatively modest number of reports on the biological applications were published. For detailed information, refer to the review of Gorbanov et al. [134]. To highlight the potential of APPJ's in bacterial disinfection and wound healing application the recent literature is discussed in the sections below. While the review articles by Keidar, Schlegel et al. and Yan et al. provide further details in the area of cancer treatment, with Kim et al. and Wu et al. providing insight into the field of dentistry [21,22,135–137].

5.1 Bacteria decontamination

Global antibiotic resistance and the increased incidence of multidrug-resistant infection has recently renewed ideas and efforts to develop a plasma device that can efficiently kill bacteria. APPJs have been one of the most used and studied configurations for this purpose. Given the unique ability of a plasma jet to produce a discharge that extends beyond the confines of the electrodes, they are the ideal tool for localised surface decontamination [138].

Until recently, very little was known about the inactivation mechanisms of cells, and most of the early research mostly resulted in the survival curves, showing the number of killed cells as a function of time-exposure. The progress and development in diagnostics techniques enabled accurate characterisation of plasma composition and quantitative measurements of individual reactive species. Such methods provide insight into the complex underlying mechanisms of APPJ mediated microbial inactivation. Reactive oxygen species (ROS), such as ozone O_3, hydroxyl radical OH·, singlet oxygen $^1O_2$, superoxide $O_2^{\cdot-}$, atomic oxygen O, organic radicals RO·, $RO_2^{\cdot}$ reactive nitrogen species (RNS), such as atomic nitrogen, N, nitric oxide $NO^{\cdot}$, nitrogen dioxide $NO_2^{\cdot}$, UV radiation, electric field and charged particles were all reported to contribute to the efficiency of plasma-assisted inactivation [139]. Each of these has

a different level of reactivity, stability, and biological function that leads to a plethora of mechanisms further complicated by the fact they can act individually, synergistically or with other systems and thus can result in broad antimicrobial activity. Numerous targets were identified in prokaryotic cells, mainly thiols, metal centres, proteins, DNA, lipids—when targeted leading to changes in membrane permeability, modification of structure and loss of activity of intracellular and extracellular protein and damages of nucleic acids [140]. When microorganisms are a subject of plasma treatment, they are simultaneously exposed to most of the plasma components, so the roles of individual species are difficult to identify. In many healthcare-related sterilisation processes, the antimicrobial properties of UV are exploited; however, early studies from Laroussi and colleagues showed that UV produced by a plasma jets does not reach sufficient doses necessary for direct microbial inactivation [132,142,143].

Reactions via reactive oxygen and nitrogen species were found to significantly contribute to the inactivation mechanisms of different microorganisms. Different approaches were carried out to explore the impact of various plasma generated RONS. Lu et al. treated *S. aureus* with an APPJ device using mixtures of He/N_2 (3%) and He/O_2 (3%) [143]. The comparison of both conditions lead to the conclusion that the ROSs, including ozone, metastable oxygen and atomic oxygen were the main reason for enhanced inactivation in the case of oxygen mixtures [143]. Similar conclusions were presented by Deng et al., who also used different proportions of O_2 in a helium APPJ to inactivate *S. aureus*. Optical emission spectroscopy revealed the increase of ROS production by the addition of 2% oxygen content in the feeding gas in comparison to pure helium [16]. Several studies focused on different oxygen admixtures as a feed gas for APPJ applications. They showed improvement in inactivation efficiency on different clinically relevant microorganisms, such as *E. coli* [144], *Pseudomonas aeruginosa* [145], *Listeria monocytogenes*, *Salmonella Typhimurium* [146], ESKAPE pathogens [147], and even viruses [148].

More in-depth investigations using different biochemical approaches (focusing on specific cell components) revealed that plasma not only generates high RONS concentrations in the gas phase but also causes accumulation of ROS inside bacterial cells. The fluorescence probe H_2DCFDA revealed the accumulation of intracellular ROS in *S. aureus* cells during APPJ treatment while the membrane stayed intact up to a particular exposure dose. After exceeding a threshold, the bacterial defence mechanisms could not neutralise the reactive products; the membrane structure showed damages and leakage leading to death [149]. Accumulation of intracellular ROS in *E. coli*, *S. aureus* and *P. aeruginosa* was also observed by Lunov et al. They showed short exposure times could trigger mechanisms similar to programmed cell death in eukaryotic cells while long exposures lead to physical damage and destruction of bacterial cells [17]. Lackmann et al. demonstrated that plasma jet generated species in addition to physical damage of cell wall also caused significant modifications of DNA and proteins [144]. When the glyceraldehyde 3-phosphate dehydrogenase (GAPDH) enzyme was used as a model protein and exposed under dry conditions, the inactivation was less efficient than when exposed in the cell environment [144].

Cells in a natural environment are typically surrounded by a moist environment, which presents a barrier for plasma species in the gaseous phase to directly attack microbial cells. ROS and RNS generated in the gaseous phase are transported through the plasma-liquid interface where the secondary RONS in liquid medium are formed. Typically, many of the strong antibacterial effects are predominantly attributed to reactions related to peroxynitrous acid, that forms under acidic conditions and degrades into OH· and NO_2· radicals [150–153]. RNSs inactivation mechanisms were suggested to be dominant in the aqueous environment and were related to intracellular nitrosative stress processes causing damage on membranes, nucleic acids and proteins [154]. Plasma liquid interactions have been gaining increased interest in the field of plasma science and technology. The intensive research is going on that complex topic and it's beyond the scope of this review. For detailed review refer to Bruggeman et al. [155].

Electric fields can also impact the viability of microorganisms. The intrinsic properties and integrity of cell membranes were observed to change when electric fields of high strengths (20 kV/cm) and in the form of short pulses (μs) were applied [156], such fields are typical in an APPJ. With a sufficiently high electric field, inactivation can occur due to reversible or irreversible membrane permeabilisation. The transmembrane potential value of 1 V is believed to be a critical threshold for breakage of the lipid bilayer. Estifaee et al. compared the effects of oxidative radicals and electric field on *E. coli* inactivation using a pulsed electric field reactor configuration [157]. They demonstrated electric field-induced extensive damages in the cell wall, and plasma generated radicals did not directly inactivate bacteria, but the presence of holes made beforehand by the electric field provoked extensive damage. Dezest et al. found similar conclusions when they treated *E. coli* with different mixtures of helium with nitrogen and oxygen [158]. According to their results, oxidative stress caused significant damage to the membrane and proteins, but the electrical field and charged particles were found to play a significant role as well [158].

Numerous Gram-positive and Gram-negative bacteria have been exposed to an APPJ yet due to the wide variation in plasma characteristics it is difficult to draw a firm conclusion on which group of bacteria is the more susceptible to plasma treatment. The tendency from most studies reported is that G- were more sensitive compared to G+ species. Helium plasma jet experiments performed by Sharkey et al. showed that G- bacterial cells of *E. coli*, *P. aeruginosa*, *K. pneumoniae* required significantly less time to reach the same level of inactivation than bacteria belonging to G+ under the same experimental conditions [159]. Several studies were in agreement with these observations [160–162].

The difference in sensitivity was linked to the cell structure differences of both groups. The cell wall of Gram-positive bacteria consists of a thick peptidoglycan layer ranging around 20–80 nm. Whereas, the cell wall of Gram-negative bacteria is thin, 8–12 nm but chemically more complex. The peptidoglycan layer location is between the plasma membrane and outer lipopolysaccharide membrane. Correlation between reduction and cell wall thickness showed that bacteria with thicker cell wall resist plasma exposure to a higher extent [163]. Direct APPJ with air as feeding gas, showed significant differences after treatment under identical experimental conditions in the morphology of *E. coli* and *S. epidermidis* cells. The cells of *E. coli* were destroyed, whereas the *S. epidermidis* cells did not show any damages [164].

The focus on biofilms in the plasma community has a recent surge of interest, and numerous studies have shown that APPJ's have the potential to be an efficient tool for elimination of biofilms. Biofilms are an assembly of microorganisms developing in extracellular polymeric substance; the latter is an arrangement of polysaccharides, proteins, lipids and extracellular DNA. The medium facilitates the development of the bacteria and protects against antibacterial agents. Typically, biofilms require longer exposure times for complete eradication compared to unprotected planktonic cells [147]. The treatment of bacteria by APPJ showed tolerance and susceptibility discrepancy between single-species biofilm and polymicrobial communities, and also in the case of ESKAPE (*Enterococcus faecium*, *Staphylococcus aureus*, *Klebsiella pneumoniae*, *Acinetobacter baumannii*, *Pseudomonas aeruginosa*, and *Enterobacter spp.*) biofilms [165].

Different penetration depths of RONS into biofilms were reported [149,166] even though few charged species and highly reactive neutrals extend beyond the plasma-sample interface. The decontamination efficacy discrepancy observed is dependent on the structure of the biofilm, the organisation of bacteria in microcolonies embedded in an extracellular matrix and connected to a surface. It is estimated that the water content of a biofilm can be as high as 90 % [167]. The complexity of the structure as well as the presence of water can both hinder and support the transport of reactive species; minimising the transmission of gaseous phase RONS whilst supporting the transport of aqueous phase species through the matrix. Regardless of the type of treatment, it has been shown that short-lived species, such as atomic oxygen, are unable to propagate beyond the liquid surface [168,169]. Despite this, reactive species such as hydroxyl radicals, hydrogen peroxide, NO_2^-/NO_3^- and peroxynitrite, can be formed in the bulk liquid through secondary reactions involving longer-lived plasma generated species. Indeed, Xiong et al. demonstrated the efficacy of a plasma jet upon a biofilm composed of 30 layers of *Porphyromonas gingivalis* (15 µm), they identified the crucial role of excited O and OH in the deactivation of the bacteria and damaging the outside membrane [166]. Xu et al. showed with a He/O_2 APPJ a reduction of bacteria population of 85% after 5 min of treatment and a depth reach of 15 µm, the cell shape was also deformed during the treatment [149].

Table 1 provides an overview of the recent literature examining the antimicrobial effect of an APPJ on various clinically relevant pathogens.

5.2 Wound healing

Chronic wounds represent a considerable burden for healthcare systems all over the world, which typically develop from burns, pressure ulcers, surgical site infections and diabetic foot ulcers. Application of low-temperature plasma to decontaminate wounds and/or stimulate healing have shown some promise in recent years, using both in vitro models as well as in vivo studies and even in clinical trials. As in the case of decontamination experiments, the use of numerous varieties of plasma sources makes it difficult to generalise the results of different research groups. Despite the effectiveness of APPJ's for the decontamination of microorganism, wound healing is a far more complex process; requiring more than just decontamination, it involves the coordination of several cellular processes, such as inflammation, hemostasis, proliferation, remodelling of collagen and angiogenesis [170]. The plasma ability to induce programmed cell death mechanism was a major motivation toward the development of plasma medicine. One of the challenges related to wound decontamination is to tailor the plasma conditions to achieve an efficient bacterial kill on one side and improved proliferation and migration of cells on the other, without causing lethal damages to the skin tissue.

Fibroblasts and keratinocytes are essential in the wound healing process, responsible for the production of collagen, which leads to the formation of rudimentary granulation tissue and of extracellular matrix (ECM). Proteases released by fibroblasts later aid the remodelling of ECM [171]. As such, they were widely used as *in vitro* cell models for wound healing, also in connection with plasma treatments. Brun et al. demonstrated that plasma generated with a helium APPJ induced proliferation and migration of fibroblast-like primary cells [172]. The plasma jet treatment promoted the fibroblast proliferation by inducing the generation of ROS and altering the cell cycle progression [20,173]

Short exposures of an argon APPJ (15 s) on murine fibroblasts cells L929 led to increased cell viability, whereas the 25 s exposure resulted in a significant reduction of viability [174]. The same cell line was also examined in the studies of Liu et al. [173] and Shi et al. [20], where improved proliferation rates after argon plasma treatment resulted in increased DNA synthesis in S phase of cell cycle. Similar improvements were observed on keratinocytes [175–177].

These studies provided evidence that increasing levels of intracellular RONS mainly cause plasma-induced proliferation and migration. In physiological conditions, RONS are generated in macrophages in the inflammation phase, when several growth factors, cytokines and enzymes are released controlling cell proliferation

and angiogenesis. Consequently, the RONS produced by plasma have the potential to influence these processes. *In vitro* cell models allow quantitative measurements of effect on specific type of cell-only and can add only a small piece to the puzzle of understanding the complex mechanisms involved in the wound healing process, where other cells and tissue components are involved. Several plasma-based studies have been done on animal models, mostly on rats [160,178–180] and mice [181,182]. Using an endoscopic based plasma system the porcine gastrointestinal tract was subjected to a CO_2 plasma jet, resulting in earlier recovery without damaging the treated region [183].

Unfortunately, no animal model can replicate human skin and human wound healing mechanisms. The argon based kiNPen developed at Leibniz Institute for Plasma Science and Technology is one of the first accredited low-temperature APPJ medical devices (class IIa) [180]. Since 2013, several plasma devices have been CE-certified, besides kiNPEn® MED; including Adtec SteriPlas (Adtec Plasma Technology, Adtec Europe, Hunslow, UK) and PlasmaDerm® (CINOGY GmbH, Duderstadt, Germany). The accreditation of APPJs has enabled the use of plasma devices on patients, with numerous treatments of infected wound and infectious skin being successfully performed [184–195].

Arndt et al. made a comparison between kINPen and Adtec SteriPlas devices, also referencing recent results [196]. The plasma treatment effectiveness was observed primarily in promoting the generation of a barrier between the wound and the environment (re-epithelialization), decreasing the size of the wound and regulating the expression of inflammatory genes [19]. A summary of suggested molecular and cellular effects initiated by plasma exposure during wound healing is detailed in Arndt [196], while the penetration of reactive species in a tissue model is presented in the review article of Szili et al. [196,197]. A summary of recent papers on the use of APPJ's used in wound healing applications is presented in Table 2.

The use of the APPJ as a tool for human treatment raises concerns over their safety. Despite the promise shown in many studies on animals and human, the relatively short term nature of these studies do not capture longer-lasting effects. Schmidt et al. conducted a follow-up risk assessment on plasma wound treatment of mice, demonstrating no destructive effect a year after the study [198]. Moreover, Metelmann et al. did a longer-term study of laser lesion treatment with a plasma jet; after a year, the observations show encouraging results and no precancerous skin [185]. Certainly the longer-term studies conducted to date show considerable promise, yet further studies and clinical trial are certainly required.

6 Conclusion/future perspectives

It is clear from this review that the APPJ is an extremely versatile tool for use in biomedical applications. Significant progress has been made over the past 2 decades to unravel the complexity involved in the interaction of non-equilibrium plasma with living tissues. Early works to uncover the nature of the plasma plume, including the physical processes driving the ionisation wave and the resulting reactive cocktail of chemical species created have paved the way to a new field of research focusing on the interaction of plasma with liquid. The use of sophisticated diagnostic techniques has highlighted the importance of the fluid dynamic interactions occurring at the plasma-gas and plasma-sample interfaces, which serve to increase the reactivity of the discharge through the entrainment of species from the background environment. Recent studies combining experimental measurements and computational modelling of an APPJ have demonstrated the power of this combined approach to uncover new insight into the interactions between the discharge, the flowing gas, and ultimately, the effect on the target. Although the simulation of transient and cumulative effects over short (ns) and long (few hundreds ms) timescales associated with kHz excited APPJs are a challenge, advances in model approaches and computational hardware mean this is now increasingly accessible. It is also clear that plasma generated RONS reaching a biological target, either directly or via a liquid medium, can elicit a wide number of different responses either through their independent interaction or through acting in synergy with other components. Increasingly sophisticated microbiological techniques have been applied to understand the impact of plasma exposure on bacteria, and now much is known about the underpinning decontamination pathways.

While significant progress has been made and it is now beyond doubt that APPJs are an excellent choice for microbial decontamination and wound healing applications, several key challenges remain. Perhaps the most pressing concern is the variability in RONS generation due to changes in environmental or sample conditions; any successful healthcare technology must be predictable and repeatable, hence future efforts should be directed towards the implementation of strategies for the continuous monitoring and control of RONS generation. While the application of sophisticated diagnostic techniques, such as laser-induced fluorescence, are unrealistic for in-situ monitoring; the application of optical emission or absorption spectroscopy is a realistic prospect to give an indication of RONS production and the day-to-day repeatability of the process. Such efforts could be further improved by comparing diagnostic data against those predicted from computational models, such as collisional-radiative models, in real-time. While monitoring the composition of RONS reaching the target is a vital first step to ensure repeatability, act-

ing on the data captured to dynamically alter the plasma generating conditions to manipulate the production of RONS remains perhaps the greatest challenge. To overcome this challenge, feedback from the sensor to the power source will be essential, yet beyond simply varying the applied voltage or frequency it is not clear how the actual composition of RONS in the plasma could be varied to negate against changes in the external environment. Recent efforts in the area of Machine Learning have certainly shown promise in safety-critical applications, where precise control of plasma parameters is a prerequisite [199]; paving the way for intelligent control of RONS generation.

Ultimately, it is clear that the use of APPJs in biomedical and healthcare applications holds enormous promise in areas of enormous clinical need. Research efforts into APPJ technology have made enormous progress, and our growing knowledge and understanding of the underpinning mechanisms the widespread adoption of APPJ technology in the clinic is becoming a real possibility.

MIH and JLW would like to thank the UK Engineering and Physical Sciences Research Council (EPSRC) for their support through Grants: EP/S025790/1, EP/R041849/1, EP/N021347/1, EP/T000104/1 and EP/S017623/1. MM would like to acknowledge the support of the Slovenian Research Agency, project J4-1770.

Author contributions

YM drafted the manuscript and conducted the experimental tests. MH, RW, ER, MM and JW provided guidance on the analysis of experimental results and insight into plasma jet characteristics. All authors contributed to the preparation of the final manuscript.

Data Availability Statement This manuscript has no associated data or the data will not be deposited. [Authors' comment: The paper is a review article and we have not generated any data.]

Appendix A: Plasma jet treatment of bacteria, virus and fungi

See Table 1.

Table 1 Overview of recent results of APPJ treatment of bacteria, virus and fungi

Target	Strain	Level of inactivation	Plasma conditions	References
Aeromonas hydrophila		> 2 log reductions after 2.5 m	Nitrogen, 10 SLM, 1 W,	[13]
Bacillus athropeus	WIS 396/3	> 3 log reductions after 5 min	Argon, 10 SLM, 27.12 MHz, 30 W	[200]
	WIS 396/3	> 2 log reductions after 3 min	Argon +0.135% O_2, 10 SLM, 27.12 MHz, 30 W	
	WIS 396/3	2.5 log reductions after 2 min	Argon + 0.135O_2+ 0.2% Nitrogen, 10 SLM, 27.12 MHz, 30 W	
Bacillus cereus spore	Clinical isolate	> 1 log reduction after 15 min	CO_2, 1 SLM, 16 kHz, 9 kV, 10 W	[201]
Bacillus subtilis	PS832	2.5 log reduction after 5 min	Argon, 10 SLM, 27.12 MHz, 30 W	[200]
	PS832	1.8 log reductions after 5 min	Argon + 0.135% O_2, 10 SLM, 27.12 MHz, 30 W	
	PS832	> 2 log reductions after 5 min	Argon + 0.135 O_2+ 0.2% Nitrogen, 10 SLM, 27.12 MHz, 30 W	
	FB122	3 log reductions after 5 min	Argon, 10 SLM, 27.12 MHz, 30 W	
	FB122	> 2.5 log reductions after 3 min	Argon + 0.135% O_2, 10 SLM, 27.12 MHz, 30 W	
	FB122	3 log reductions after 3 min	Argon + 0.135 O_2+ 0.2% Nitrogen, 10 SLM, 27.12 MHz, 30 W	
	PS578	> 3 log reductions after 1 min	Argon, 10 SLM, 27.12 MHz, 30 W	
	PS578	5 log reductions after 3 min	Argon + 0.135% O, 10 SLM, 27.12 MHz, 30 W	
Escherichia coli		Observable sterilization effect	IIelium, Microplasma 3 × 3 array, 02 kV, 20 kHz	[19]
		> 8 log reductions after 9 min	Argon, PTFE channel 1200 mm or 2200 mm, 10 kV, 15.9 W, 23 kHz	[48]
		> 4 log reductions after 7 min	Air, Plasma-activated media, pH 3.3, 27 kV, 50 Hz pulse rep,	[202]
		> 3 log reductions after 15 min	Argon/O_2, Plasma-activated media, 27 kV, 50 Hz pulse rep, pH 10.1	
	ATCC25922	> 6 log reductions after 30 s	CO_2 , 1 SLM, 16 kHz, 9 kV, 10 W	[201]
	DSM 11250	> 6 log reductions after 1 min	Nitrogen, 1 SLM, 16 kHz, 9 kV, 10 W	
	DSM 11250	> 3 log reductions after 2 min	Argon, 20 SLM, 20 W, 27.12 Mhz,	[203]
		> 4 log reductions after 1 min	Argon, 20 SLM, 20 W, 27.12 Mhz,	
	O157:H7	> 1 log reductions after 2.5 min	Nitrogen, 10 SLM, 1 W,	[13]
	O157: H7 strain CICC 10907	> 3 log reductions after 6 min	Air, Plasma-activated water, 60 s, 200 mL distilled water, 750 W	[204]
	DH5	> 4 log reductions after 150 s	Helium, 5E-6 m^3/s, 16 kV,	[205]
	DH5	> 5 log reductions after 150 s	Argon, 5E-6 m^3/s, 16 kV,	
	DH5	> 6 log reductions after 150 s	Air, 5E-6 m^3/s, 16 kV,	
	DH5	> 7 log reductions after 150 s	Helium + Air, 5E-6 m^3/s,16 kV,	
		> 20% reduction after 1 min	Helium, 1 L min^{-1}, 9.6 kV, 9.5 kHz	[206]
		> 95% reduction after 1 min	Helium, 1 L min^{-1}, 9.6 kV, 9.5 kHz, 100 μM KI(Potassium Iodide)	
	ATCC25922	8 log reductions after 8 min	Argon, 1 L min^{-1}, 50 W, RF	[207]
	ATCC25922	4 log reductions after 8 min	Argon, 1 L min^{-1}, 20 W, RF	
	K12	> 0 log reductions after 11.5 min	Argon + O_2 (1%), 4 SLM, C-DBD, 15 kVpp, 20 kHz	[208]
	K12	> 7 log reductions after 6.5 min	Argon, 3 SLM, Plasma underwater, 6.8 kVpp, 1.5 kHz	
	K12	> 1 log reduction after 1 min	Helium 2 SLM + O_2 0.01 SLM, 17–20 kVpp, 5 kHz	[209]
		> 6 log reductions after 100 s	Helium + O_2(0.2%), 14 L min^{-1}, 3.5 kV, 20 kHz	[210]
		> 5 log reductions after 100 s	Helium, 14 L min^{-1}, 3.5 kV, 20 kHz	[210]
		> 5 log reductions after 100 s	Helium + N_2(0.2%), 14 L min^{-1}, 3.5 kV, 20 kHz	[210]
	DSM 1103	> 5 log reductions after 2 min	kINPen Vet-NeoPlas, Ar, 5 SLM, 3 kV, 1 MHz	[211]
Enterococcus faecalis	ATCC29212	> 6 log reductions after 1 min	CO_2,1 SLM, 16 kHz, 9 kV, 10 W	[201]
	ATCC29212	> 6 log reductions after 1 min	Nitrogen, 1 SLM, 16 kHz, 9 kV, 10 W	
Listeria innocua		> 3 log reductions after 2 min	Nitrogen, 10 SLM, 1 W,	[13]
Listeria monocytogenes		> 3 log reductions after 2 min	Nitrogen, 10 SLM, 1 W,	[13]

Table 1 continued

Target	Strain	Level of inactivation	Plasma conditions	References
MRSA	Clinical isolate	> 6 log reductions after 1 min	CO_2, 1 SLM, 16 kHz, 9 kV, 10 W	[201]
	Clinical isolate	> 6 log reductions after 30 s	Nitrogen, 1 SLM, 16 kHz, 9 kV, 10 W	
Mycobacterium abscessus	ATCC19977	2 log reductions after 10 min	CO_2, 1 SLM, 16 kHz, 9 kV, 10 W	[201]
	ATCC19977	> 6 log reductions after 1 min	Nitrogen, 1 SLM, 16 kHz, 9 kV, 10 W	
Mycobacterium terrae	JCM12143	1 log reductions after 10 min	CO_2, 1 SLM, 16 kHz, 9 kV, 10 W	[201]
	JCM12143	> 6 log reductions after 10 min	Nitrogen, 1 SLM, 16 kHz, 9 kV, 10 W	
Planktonic bacteria	PA14	> 9 log reductions after 2 min	Argon + 1% O_2, Direct treatment in saline solution	[18]
	PA14	> 9 log reductions after 2.5 min	Argon + 1% Air, Direct treatment in saline solution	
	PA14	> 5 log reductions after 3 min	Argon, Direct treatment in saline solution	
	PA14	> 9 log reductions after 3 min	Argon + 1% O_2, Indirect treatment in saline solution	
	PA14	> 9 log reductions after 3 min	Argon + 1% Air, Indirect treatment in saline solution	
	PA14	< 1 log reduction after 3 min	Argon, Indirect treatment in saline solution	
	PA14	> 9 log reductions after 3 min	Argon + 1% O_2, Direct treatment in distilled water	
	PA14	> 3 log reductions after 3 min	Argon + 1% Air, Direct treatment in distilled water	
	PA14	> 6 log reductions after 3 min	Argon, Direct treatment in distilled water	
Plesiomonas shigelloides		> 1 log reduction after 2.5 min	Nitrogen, 10 SLM, 1 W	[13]
Pseudomonas aeruginosa		> 8 log reductions after 9 min	Argon, PTFE channel 1200 mm or 2200 mm, 10 kV, 15.9 W, 23 kHz	[48]
	ATCC27853	> 6 log reductions after 30 s	CO_2, 1 SLM, 16 kHz, 9 kV, 10 W	[201]
	ATCC27853	> 6 log reductions after 1 min	CO_2or Nitrogen, 1 SLM, 16 kHz, 9 kV, 10 W	
	ATCC27853	< 1 log reduction after 2 min	Mock air or Argon or O_2, 1 SLM, 16 kHz, 9 kV, 10 W	
		> 50% reduction after 1 min	Helium, 1 L min^{-1}, 9.6 kV, 9.5 kHz	[206]
		> 95% reduction after 1 min	Helium, 1 L min^{-1}, 9.6 kV, 9.5 kHz, 100 μM KI(Potassium Iodide)	
	DSM 1117	> 5 log reductions after 2 min	kINPen Vet-NeoPlas, Ar, 5 SLM, 3 kV, 1 MHz	[211]
Pseudomonas deceptionensis	CM2	~ 5 log reductions after 10 min	Air, Plasma-activated water, 60 s, 200 mL distilled water, 750 W	[204]
Saccharomyces cerevisiae	YPH250	> 90% reductions after 25 min	Argon, 0.8 SLM, 20 kV, 11 kHz,	[212]
Salmonella enterica serovar typhimurium		> 2 log reductions after 2.5 min	Nitrogen, 10 SLM, 1 W,	[13]
Salmonella enterica serovar enteritidis		> 1 log reduction after 2.5 min	Nitrogen, 10 SLM, 1 W,	[13]
Staphylococcus aureus		> 2 log reductions after 1 min	Helium, 4 SLM, 12 kHz, 7.5 kVp-p	[141]
		> 8 log reductions after 9 min	Argon, PTFE channel 1200 mm or 2200 mm, 10 kV, 15.9 W, 23 kHz	[48]
	ATCC25923	> 6 log reductions after 1 min	CO_2 or Nitrogen, 1 L/min, 16 kHz, 9 kV, 10 W	[201]
	ATCC25923	3 log reductions after 2 min	O_2, 1 SLM, 16 kHz, 9 kV, 10 W	
	ATCC25923	< 1 log reduction after 2 min	Mock air, Argon, 1 SLM, 16 kHz, 9 kV, 10 W	
		> 7 log reductions after 15 min	O_2, 2.5 L/h, 21 kV, 30 mA, 650 Hz, direct treatment in liquid	[213]

Table 1 continued

Target	Strain	Level of inactivation	Plasma conditions	References
		> 7 log reductions after 25 min	Air, 2.5 L/h, 21 kV, 30 mA, 650 Hz, direct treatment in liquid	
		> 1 log reduction after 350 min	O_2, 2.5 L/h, 21 kV, 30 mA, 650 Hz, indirect treatment in liquid	
		> 5 log reductions after 350 min	Air, 2.5 L/h, 21 kV, 30 mA, 650 Hz, indirect treatment in liquid	
		> 2 log reductions after 2 min	Nitrogen, 10 SLM, 1 W,	[13]
	GIM1.441	> 3 log reductions after 6 min	Air, Plasma-activated water, 60 s, 200 mL distilled water, 750 W	[204]
		> 80% reduction after 40 s	Helium, 1 L min^{-1}, 9.6 kV, 9.5 kHz	[206]
		> 95% reduction after 40 s	Helium, 1 L min^{-1}, 9.6 kV, 9.5 kHz, 100 μM KI(Potassium Iodide)	
	ATCC12600	> 2 log reductions after 11.5 min	Argon + O_2 (1%), 4 SLM, C-DBD, 15 kVpp, 20 kHz	[208]
	ATCC12600	3 log reductions after 6.5 min	Argon, 3 SLM, Plasma underwater, 6.8 kVpp, 1.5 kHz	[208]
	USA300 JE2	> 1 log reduction after 1 min	Helium 2 SLM + O_2 0.01 SLM, 17–20 kVpp, 5 kHz	[209]
	DSM 1104	> 4 log reductions after 2 min	kINPen Vet-NeoPlas, Ar, 5 SLM, 3 kV, 1 MHz	[211]
feline calicivirus F9		5 log reductions after 1 min	CO_2, 1 SLM, 16 kHz, 9 kV, 10 W	[201]
		> 6 log reductions after 3 min	Nitrogen, 1 SLM, 16 kHz, 9 kV, 10 W	
	Strain 255	> 5 log reductions after 5 min	Argon, 13.56 MHz, modulated freq 20 kHz, 2.5 W	[148]
	Strain 255	> 6 log reductions after 2 min	Argon + 1% O_2, 13.56 MHz, modulated freq 20 kHz, 2.5 W	
	Strain 255	> 6 log reductions after 3 min	Argon + 1% Air, 13.56 MHz, modulated freq 20 kHz, 2.5 W	
	Strain 255	> 3 log reductions after 5 min	Argon + 0.27% water plasma 13.56 MHz, modulated freq 20 kHz, 2.5 W	
RNA viruses coxsackievirus A7		2 log reductions after 10 min	CO_2, 1 SLM, 16 kHz, 9 kV, 10 W	[201]
Aspergillus niger	NBRC105649	> 1 log reduction after 10 min	CO_2, 1 SLM, 16 kHz, 9 kV, 10 W	[201]
	NBRC105649	> 6 log reductions after 5 min	Nitrogen, 1 SLM, 16 kHz, 9 kV, 10 W	
Candida albicans		Remarkable decrease at 1.5 min	Helium, Microplasma 3 × 3 array, 2 kV, 20 kHz	[19]
	NBRC15943	5 log reductions after 1 min	CO_2, 1 SLM, 16 kHz, 9 kV, 10 W	[201]
	NBRC15943	> 6 log reductions after 1 min	Nitrogen, 1 SLM, 16 kHz, 9 kV, 10 W	
	SC 5314	> 90% reductions after 150 s	Helium, 2 SLM, 1.8 W,	[214]

Appendix B: Plasma jet treatment of animal and human wounds

See Table 2.

Table 2 Overview of recent results of APPJ treatment of animal and human wounds

Target	Plasma conditions	Treatment (Frequency, period, exposure)	Reference
Wild-type mouse	Ar, 4 SLM, 110 W, 2.45 GHz	Once a day, 10 days, 2 min	[181]
Diabetic mice	CAP Med, He, 10.8 SLM, 7 kVpp, 17 kHz	15 s	[215]
Male Balb/c mice	He, 0.5–2 SLM, 30 kVpp, 10–12 kHz	10–50 s	[216]
	Ar, 2 L/m, 8 kVpp, 37.5 kHz	Once a day, 14 days, 10–50 s	[217]
	Ar, 2 SLM, 8 kVpp, 37.5 kHz	Once a day, 14 days	[20]
	Ar, 1 SLM, 9.58 kV, 55.2 mA, 18.32 kHz	1–5 min, 14 days	[218]
	Ar, 5 SLM, 25 kV, 20 kHz	Once a day, 15 days, 1 min	[219]
SKH1-hr mice	kINPen 11 neoplas tool, Ar, 5 SLM, 1 MHz,	Once a day, 14 days, 20 s	[198]
Male Sprague–Dawley rats	Ar/O2, 1.8/0.01 L/min, 0.5–4 kHz,	Once a day, 4 weeks, 5 min	[220]
	Arrays, He, 0.35–1.5 SLM, 20 kHz, 3–96 mW	Twice a day, 5 days	[19]
	Ar/O2/H2O, 5 SLM, 0–20 kVpp, 20–25 kHz, 60 W	Once per day, 90 s	[221]
Male Wistar rats	Ar, 2.5 SLM, 9–15 kV, 5 kHz,	30 times a day, 4 days, 60 s	[222]
	Air, 4 SLM, 0.6 kV, 200 kHz,	Thrice a day, 3–7–14 days, 3 min	[178]
	He, 4 SLM, 5 kVpp, 25 kHz	Thrice a day, 5 days, 60 s	[179]
Diabetic rat	Ar, 5 SLM, 20 kHz,	Once a day, 120–240 s	[223]
Rat skin	Air, 4 SLM, 0.6 kV, 200 kHz,	2 min	[224]
	He, 1000 sccm, 10 kV, 20 kHz	5 min	[225]
Pig intestinal	Ar, He, O, N, Air, CO2, 1 L/m, 50 Hz, 2.25 kV	Until hemostasis	[226]
Sheep skin	He, 1.75 L min^{-1}, 1 kVpp , RF 5 MHz,	Once a day, 2 min,	[227]
Chronic infected human skin wound	MicroPlaSter alpha device, Ar, 2.2 SLM, 2.46 GHz, 86 W,	2 min	[193]
	MicroPlaSter beta device, Ar, 2.2 SLM, 2.46 GHz, 86 W,	2 min	[193]
Radial forearm skin	PlasmaDerm® FLEX9060 CINOGY GmbH, 300 Hz, 10 kV, 450 mW	3 x 90 s	[228]
Laser lesions on human skin	kINPen® MED Neoplas GmbH, Ar,4–6 SLM,2–3 kVpp, 1 MHz	Once a day, 10, 30, 3 × 10 s	[185]
Human tissue	kINPen® MED Neoplas GmbH, Ar, 4 SLM, 1.1 MHz,	3–120 s	[229]
Human forearm wound	kINPen® MED Neoplas GmbH, Ar,4–6 SLM, 1.82 MHz	Once a day, 6 days, 60 s	[187]
Human chronic leg ulcer	kINPen 09, Ar, 5 SLM, 3 W, 1.82 MHz	2 min	[195]
Human pressure ulcer	Ar, 50 W, 50 Hz pulse rep	Once a week, 8 weeks	[189]
Human venous leg ulcers	PlasmaDerm VU-2010, Air, 50 Hz, 120 mW/cm2	Thrice a week, 8 weeks, 2 × 45 s	[188]
Human exposed flexor tendons	kINPen® MED Neoplas GmbH, Ar,4–6 SLM, 1 MHz	Ten times a week, 6–16 weeks	[190]

References

1. A. Fridman, Plasma Chemistry (2008) Cambridge University Press, UK
2. M. Laroussi, IEEE Trans. Plasma Sci. **24**(3), 1188–1191 (1996). https://doi.org/10.1109/27.533129
3. D.B. Graves, J. Phys. D. Appl. Phys. **45**, 26 (2012). https://doi.org/10.1088/0022-3727/45/26/263001
4. M.H. Qaisrani, Y. Xian, C. Li, X. Pei, M. Ghasemi, X. Lu, Phys. Plasmas **23**, 6 (2016). https://doi.org/10.1063/1.4954828
5. E. Robert, V. Sarron, T. Darny, D. Riès, S. Dozias, J. Fontane, L. Joly, J.-M. Pouvesle, Plasma Sources Sci. Technol. **23**(1), 12003 (2014). https://doi.org/10.1088/0963-0252/23/1/012003
6. M. Boselli, V. Colombo, E. Ghedini, M. Gherardi, R. Laurita, A. Liguori, P. Sanibondi, A. Stancampiano, Plasma Chem. Plasma Process. **34**(4), 853–869 (2014). https://doi.org/10.1007/s11090-014-9537-1
7. J.W. Bradley, J.S. Oh, O.T. Olabanji, C. Hale, R. Mariani, K. Kontis, IEEE Trans. Plasma Sci. **39**(11 PART 1), 2312–2313 (2011). https://doi.org/10.1109/TPS.2011.2157940
8. R.D. Whalley, J.L. Walsh, Sci. Rep. **6**(1), 1–11 (2016). https://doi.org/10.1038/srep31756
9. Y. Morabit, R.D. Whalley, E. Robert, M.I. Hasan, J.L. Walsh, Plasma Process. Polym. (2019). https://doi.org/10.1002/ppap.201900217
10. E. Gutmark, C.M. Ho, Phys. Fluids **26**(10), 2932–2938 (1983). https://doi.org/10.1063/1.864058
11. H. Sato, J. Phys. Soc. Japan **14**(12), 1797–1810 (1959). https://doi.org/10.1143/JPSJ.14.1797
12. A. Michalke, J. Fluid Mech. **23**(3), 521–544 (1965). https://doi.org/10.1017/S0022112065001520
13. S. Colejo, A. Alvarez-ordóñez, M. Prieto, M. López, Innov. Food Sci. Emerg. Technol. **50**(October), 84–93 (2018). https://doi.org/10.1016/j.ifset.2018.10.002
14. M. Rossow, M. Ludewig, P.G. Braun, LWT Food Sci. Technol **91**(April 2017), 265–270 (2018). https://doi.org/10.1016/j.lwt.2018.01.052
15. A. Shaw, G. Shama, F. Iza, A. Shaw **029402**, (2015). https://doi.org/10.1116/1.4914029
16. G. Deng, Q. Jin, S. Yin, C. Zheng, Z. Liu, K. Yan (2018)
17. O. Lunov, V. Zablotskii, O. Churpita, A. Jäger, L. Polívka, E. Syková, A. Dejneka, Š. Kubinová, Biomaterials **82**, 71–83 (2016). https://doi.org/10.1016/j.biomaterials.2015.12.027
18. V.S.S.K. Kondeti, C.Q. Phan, K. Wende, H. Jablonowski, U. Gangal, J.L. Granick, R.C. Hunter, P.J. Bruggeman, Free Radic. Biol. Med. **124**(May), 275–287 (2018). https://doi.org/10.1016/j.freeradbiomed.2018.05.083
19. O.J. Lee, H.W. Ju, G. Khang, P.P. Sun, J. Rivera, J.H. Cho, S. Park, J.G. Eden, C.H. Park, (July 2015) 348–57 (2016) . https://doi.org/10.1002/term
20. X. Shi, G. Xu, G. Zhang, J. Liu **38**, 1 (2018)
21. M. Keidar, Plasma Sources Sci. Technol. **24**, 3 (2015). https://doi.org/10.1088/0963-0252/24/3/033001
22. J. Schlegel, J. Köritzer, V. Boxhammer, Clin. Plasma Med. **1**(2), 2–7 (2013). https://doi.org/10.1016/j.cpme.2013.08.001
23. S. Bekeschus, P. Favia, E. Robert, T. von Woedtke, Plasma Process. Polym. **16**(1), 1–12 (2019). https://doi.org/10.1002/ppap.201800033
24. V. Miller, A. Lin, A. Fridman, Plasma Chem. Plasma Process. **36**(1), 259–268 (2016). https://doi.org/10.1007/s11090-015-9676-z
25. M. Vandamme, E. Robert, S. Pesnel, E. Barbosa, S. Dozias, J. Sobilo, S. Lerondel, A. Le Pape, J.M. Pouvesle, Plasma Process. Polym. **7**(3–4), 264–273 (2010). https://doi.org/10.1002/ppap.200900080
26. T. Von Woedtke, H.R. Metelmann, K.D. Weltmann, Contrib. Plasma Phys. **54**(2), 104–117 (2014). https://doi.org/10.1002/ctpp.201310068
27. H.R. Metelmann, C. Seebauer, V. Miller, A. Fridman, G. Bauer, D.B. Graves, J.M. Pouvesle, R. Rutkowski, M. Schuster, S. Bekeschus, K. Wende, K. Masur, S. Hasse, T. Gerling, M. Hori, H. Tanaka, E. Ha Choi, K.D. Weltmann, P.H. Metelmann, D.D. Von Hoff, T. von Woedtke, Clin. Plasma Med **9**, 6–13 (2018). https://doi.org/10.1016/j.cpme.2017.09.001
28. M. Laroussi, T. Akan, Plasma Process. Polym. **4**(9), 777–788 (2007). https://doi.org/10.1002/ppap.200700066
29. X. Lu, M. Laroussi, V. Puech (2012). https://doi.org/10.1088/0963-0252/21/3/034005
30. X. Lu, G.V. Naidis, M. Laroussi, K. Ostrikov, Phys. Rep. **540**(3), 123–166 (2014). https://doi.org/10.1016/j.physrep.2014.02.006
31. K.D. Weltmann, E. Kinde, T. Von Woedtke, M. Hähnel, M. Stieber, R. Brandenburg, Pure Appl. Chem. **82**(6), 1223–1237 (2010). https://doi.org/10.1351/PAC-CON-09-10-35
32. M. Laroussi, IEEE Trans. Plasma Sci. **37**(6 PART 1), 714–725 (2009). https://doi.org/10.1109/TPS.2009.2017267
33. W. Gong, Y. Yue, F. Ma, F. Yu, J. Wan, L. Nie, K. Bazaka, Y. Xian, X. Lu, K. Ostrikov, Phys. Plasmas **25**, 1 (2018). https://doi.org/10.1063/1.5010993
34. R. Wang, Y. Gao, C. Zhang, P. Yan, T. Shao, IEEE Trans. Plasma Sci. **44**(4), 393–397 (2016). https://doi.org/10.1109/TPS.2016.2521826
35. T. Shao, C. Zhang, R. Wang, Y. Zhou, Q. Xie, Z. Fang, IEEE Trans. Plasma Sci. **43**(3), 726–732 (2015). https://doi.org/10.1109/TPS.2014.2359515
36. E.J. Baek, H.M. Joh, S.J. Kim, T.H. Chung, Phys. Plasmas **23**, 7 (2016). https://doi.org/10.1063/1.4959174
37. X. Pei, M. Ghasemi, H. Xu, Q. Hasnain, S. Wu, Y. Tu, X. Lu, Plasma Sources Sci. Technol. **25**(3), 035013 (2016). https://doi.org/10.1088/0963-0252/25/3/035013
38. H.R. Kang, T.H. Chung, H.M. Joh, S.J. Kim, IEEE Trans. Plasma Sci. **45**(4), 691–697 (2017). https://doi.org/10.1109/TPS.2017.2678527
39. C. Canal, R. Fontelo, I. Hamouda, J. Guillem-Marti, U. Cvelbar, M.P. Ginebra, Free Radic. Biol. Med. **110**(December 2016), 72–80 (2017). https://doi.org/10.1016/j.freeradbiomed.2017.05.023
40. K. Yambe, H. Saito, J. Phys. Soc. Japan **86**(12), 1–5 (2017). https://doi.org/10.7566/JPSJ.86.124502
41. Y. Xia, W. Wang, D. Liu, W. Yan, Z. Bi, L. Ji, J. Niu, Y. Zhao, Phys. Plasmas **25**(2), 2–7 (2018). https://doi.org/10.1063/1.5009127
42. G.V. Naidis, J.L. Walsh, J. Phys. D. Appl. Phys. **46**, 095203 (2013). https://doi.org/10.1088/0022-3727/46/9/095203

43. P.K. Papadopoulos, P. Vafeas, P. Svarnas, K. Gazeli, P.M. Hatzikonstantinou, A. Gkelios, F. Clément, J. Phys. D. Appl. Phys. **47**, 42 (2014). https://doi.org/10.1088/0022-3727/47/42/425203
44. S. Mirpour, H. Ghomi, S. Piroozmand, M. Nikkhah, IEEE Trans. Plasma Sci. **42**(2), 315–322 (2014). https://doi.org/10.1109/TPS.2013.2291860
45. M. Engelhardt, R. Pothiraja, K. Kartaschew, N. Bibinov, M. Havenith, P. Awakowicz, J. Phys. D. Appl. Phys. **49**(14), 145201 (2016). https://doi.org/10.1088/0022-3727/49/14/145201
46. Q. Xiang, C. Kang, L. Niu, D. Zhao, K. Li, Y. Bai, Lwt **96**(136), 395–401 (2018). https://doi.org/10.1016/j.lwt.2018.05.059
47. K. Urabe, Y. Ito, O. Sakai, K. Tachibana, Jpn. J. Appl. Phys. **49**(10), 1060011–6 (2010). https://doi.org/10.1143/JJAP.49.106001
48. S. Bhatt, P. Mehta, C. Chen, C.L. Schneider, L.N. White, H.L. Chen, M.G. Kong, Gastrointest. Endosc. **89**(1), 105–114 (2019). https://doi.org/10.1016/j.gie.2018.08.009
49. K.G. Kostov, M. Machida, V. Prysiazhnyi, R.Y. Honda, Plasma Sources Sci. Technol. **24**, 2 (2015). https://doi.org/10.1088/0963-0252/24/2/025038
50. G. Cho, Y. Kim, H.S. Uhm, J. Korean Phys. Soc. **69**(4), 525–535 (2016). https://doi.org/10.3938/jkps.69.525
51. E. Robert, E. Barbosa, S. Dozias, M. Vandamme, C. Cachoncinlle, R. Viladrosa, J.M. Pouvesle, Plasma Process. Polym. **6**(12), 795–802 (2009). https://doi.org/10.1002/ppap.200900078
52. J. Winter, T.M.C. Nishime, S. Glitsch, H. Lühder, K.D. Weltmann, Contrib. Plasma Phys. **58**(5), 404–414 (2018). https://doi.org/10.1002/ctpp.201700127
53. J. Winter, T.M.C. Nishime, R. Bansemer, M. Balazinski, K. Wende, K.D. Weltmann, J. Phys. D. Appl. Phys. **52**, 2 (2019). https://doi.org/10.1088/1361-6463/aae817
54. J.Y. Kim, J. Ballato, P. Foy, T. Hawkins, Y. Wei, J. Li, S.O. Kim, Small **6**(14), 1474–1478 (2010). https://doi.org/10.1002/smll.201000480
55. J.Y. Kim, Y. Wei, J. Li, P. Foy, T. Hawkins, J. Ballato, S.O. Kim, Small **7**(16), 2291–2295 (2011). https://doi.org/10.1002/smll.201100456
56. Z. Xiong, M.J. Kushner, Plasma Sources Sci. Technol. **21**, 3 (2012). https://doi.org/10.1088/0963-0252/21/3/034001
57. F. Judée, N. Merbahi, G. Wattieaux, M. Yousfi, J. Appl. Phys. **120**, 11 (2016). https://doi.org/10.1063/1.4961037
58. S. Bekeschus, A. Schmidt, K.D. Weltmann, T. von Woedtke, Clin. Plasma Med. **4**(1), 19–28 (2016). https://doi.org/10.1016/j.cpme.2016.01.001
59. Q.Y. Nie, Z. Cao, C.S. Ren, D.Z. Wang, M.G. Kong, New J. Phys. **11** (2009). https://doi.org/10.1088/1367-2630/11/11/115015
60. M. Ghasemi, P. Olszewski, J.W. Bradley, J.L. Walsh, J. Phys. D. Appl. Phys. **46**, 5 (2013). https://doi.org/10.1088/0022-3727/46/5/052001
61. Z. Fang, Z. Ding, T. Shao, C. Zhang, IEEE Trans. Dielectr. Electr. Insul. **23**(4), 2288–2293 (2016). https://doi.org/10.1109/TDEI.2016.7556505
62. X. Cui, B. Yan, B. Zhang, Z. Fang, Vacuum **151**, 15–24 (2018). https://doi.org/10.1016/j.vacuum.2018.01.042
63. H.J. Park, S.H. Kim, H.W. Ju, H. Lee, Y. Lee, S. Park, H. Yang, S.-J. Park, J.G. Eden, J. Yang, C.H. Park, Sci. Rep. **8**(1), 2422 (2018). https://doi.org/10.1038/s41598-018-20854-8
64. T. Wang, X. Wang, B. Yang, X. Chen, C. Yang, J. Liu, J. Micromechanics Microengineering **27**, 7 (2017). https://doi.org/10.1088/1361-6439/aa703a
65. M. Wan, F. Liu, Z. Fang, B. Zhang, H. Wan, Phys. Plasmas **24**, 9 (2017). https://doi.org/10.1063/1.4991531
66. E. Robert, T. Darny, S. Dozias, S. Iseni, J.M. Pouvesle, Phys. Plasmas **22**, 12 (2015). https://doi.org/10.1063/1.4934655
67. A.M. Lietz, X. Damany, E. Robert, J.-M. Pouvesle, M.J. Kushner, Plasma Sources Sci. Technol. **28**(12), 125009 (2019). https://doi.org/10.1088/1361-6595/ab4ab0
68. J.S. Oh, O.T. Olabanji, C. Hale, R. Mariani, K. Kontis, J.W. Bradley, J. Phys. D. Appl. Phys. **44**, 15 (2011). https://doi.org/10.1088/0022-3727/44/15/155206
69. S. Park, U. Cvelbar, W. Choe, S.Y. Moon, Nat. Commun. **9**, 1 (2018). https://doi.org/10.1038/s41467-017-02766-9
70. Z. Chen, G. Xia, C. Zou, X. Liu, D. Feng, P. Li, Y. Hu, O. Stepanova, A.A. Kudryavtsev, J. Appl. Phys. **122**, 9 (2017). https://doi.org/10.1063/1.5001247
71. M. Teschke, J. Kedzierski, E.G. Finantu-Dinu, D. Korzec, J. Engemann, IEEE Trans. Plasma Sci. **33**(2 I), 310–311 (2005). https://doi.org/10.1109/TPS.2005.845377
72. G.V. Naidis, J. Phys. D. Appl. Phys. **43**, 40 (2010). https://doi.org/10.1088/0022-3727/43/40/402001
73. G.V. Naidis, J. Phys. D. Appl. Phys. **44**(21), 215203 (2011). https://doi.org/10.1088/0022-3727/44/21/215203
74. J.P. Boeuf, L.C. Pitchford, Phys. Rev. E **51**(2), 1376–1390 (1995). https://doi.org/10.1103/PhysRevE.51.1376
75. D. Breden, K. Miki, L.L. Raja, Appl. Phys. Lett. **99**, 11 (2011). https://doi.org/10.1063/1.3636433
76. D. Breden, K. Miki, L.L. Raja, Plasma Sources Sci. Technol. **21**, 3 (2012). https://doi.org/10.1088/0963-0252/21/3/034011
77. J.P. Boeuf, L.L. Yang, L.C. Pitchford, J. Phys. D. Appl. Phys. **46**, 1 (2013). https://doi.org/10.1088/0022-3727/46/1/015201
78. E. Robert, V. Sarron, D. Riès, S. Dozias, M. Vandamme, J.-M. Pouvesle, Plasma Sources Sci. Technol. **21**(3), 034017 (2012). https://doi.org/10.1088/0963-0252/21/3/034017
79. R. Ye, W. Zheng, Appl. Phys. Lett. **93**(7), 1–4 (2008). https://doi.org/10.1063/1.2972119
80. D. Maletić, N. Puač, N. Selaković, S. Lazović, G. Malović, A. Dordević, Z.L. Petrović, Plasma Sources Sci. Technol. **24**, 2 (2015). https://doi.org/10.1088/0963-0252/24/2/025006
81. Z. Xiong, E. Robert, V. Sarron, J.M. Pouvesle, M.J. Kushner, J. Phys. D. Appl. Phys. **45**, 27 (2012). https://doi.org/10.1088/0022-3727/45/27/275201
82. G.B. Sretenović, I.B. Krstić, V.V. Kovačević, B.M. Obradović, M.M. Kuraica, J. Phys. D. Appl. Phys. **47**, 10 (2014). https://doi.org/10.1088/0022-3727/47/10/102001
83. V.V. Kovačević, G.B. Sretenović, E. Slikboer, O. Guaitella, A. Sobota, M.M. Kuraica, J. Phys. D.

Appl. Phys. **51**, 6 (2018). https://doi.org/10.1088/1361-6463/aaa288
84. A. Bourdon, T. Darny, F. Pechereau, J.-M. Pouvesle, P. Viegas, S. Iséni, E. Robert, Plasma Sources Sci. Technol. **25**(3), 035002 (2016). https://doi.org/10.1088/0963-0252/25/3/035002
85. A. Sobota, O. Guaitella, G.B. Sretenović, I.B. Krstić, V.V. Kovačević, A. Obrusník, Y.N. Nguyen, L. Zajíčková, B.M. Obradović, M.M. Kuraica, Plasma Sources Sci. Technol. **25**, 6 (2016). https://doi.org/10.1088/0963-0252/25/6/065026
86. F. Liu, D. Zhang, D. Wang, Thin Solid Films **521**, 261–264 (2012). https://doi.org/10.1016/j.tsf.2011.10.200
87. A. Begum, M. Laroussi, M.R. Pervez, AIP Adv. **3**, 6 (2013). https://doi.org/10.1063/1.4811464
88. R. Wang, K. Zhang, Y. Shen, C. Zhang, W. Zhu, T. Shao, Plasma Sources Sci. Technol. **25**, 1 (2016). https://doi.org/10.1088/0963-0252/25/1/015020
89. P. Olszewski, E. Wagenaars, K. McKay, J.W. Bradley, J.L. Walsh, Plasma Sources Sci. Technol. **23**, 1 (2014). https://doi.org/10.1088/0963-0252/23/1/015010
90. R.P. Joshi, V. Sridhara, K.H. Schoenbach, Biochem. Biophys. Res. Commun. **348**(2), 643–648 (2006). https://doi.org/10.1016/j.bbrc.2006.07.144
91. S.A. Norberg, E. Johnsen, M.J. Kushner, J. Phys. D. Appl. Phys. **49**(18), 185201 (2016). https://doi.org/10.1088/0022-3727/49/18/185201
92. P. Zhu, Z. Meng, H. Hu, J. Ouyang, Phys. Plasmas **24**, 10 (2017). https://doi.org/10.1063/1.5004419
93. L. Lin, M. Keidar, Phys. Plasmas **23**, 8 (2016). https://doi.org/10.1063/1.4961924
94. E. Robert, V. Sarron, D. Riès, S. Dozias, M. Vandamme, J.M. Pouvesle, Plasma Sources Sci. Technol. **21**, 3 (2012). https://doi.org/10.1088/0963-0252/21/3/034017
95. J.L. Walsh, P. Olszewski, J.W. Bradley, Plasma Sources Sci. Technol. **21**, 3 (2012). https://doi.org/10.1088/0963-0252/21/3/034007
96. M.I. Hasan, J.W. Bradley, J. Phys. D. Appl. Phys. **48**, 43 (2015). https://doi.org/10.1088/0022-3727/48/43/435201
97. M. Qian, C. Yang, S. Liu, X. Chen, G. Ni, D. Wang, Jpn. J. Appl. Phys. **55**, 4 (2016). https://doi.org/10.7567/JJAP.55.046101
98. M. Liang, Y. Liang, J. Chai, S. Zhou, J. Jiang **79**(11), 2308–2314 (2014). https://doi.org/10.1111/1750-3841.12660
99. J.S. Oh, J.L. Walsh, J.W. Bradley, Plasma Sources Sci. Technol. **21**, 3 (2012). https://doi.org/10.1088/0963-0252/21/3/034020
100. J.P. Boeuf, L.C. Pitchford, J. Appl. Phys. **97**, 10 (2005). https://doi.org/10.1063/1.1901841
101. M.I. Hasan, J.W. Bradley, J. Phys. D. Appl. Phys. **49**, 5 (2015). https://doi.org/10.1088/0022-3727/49/5/055203
102. C.J. Chen, W. Rodi, *Vertical Turbulent Buoyent Jets: A Review of Experimental Data* (Pergamon Press, Oxford, 1980)
103. G.K. Batchelor, A.E. Gill, J. Fluid Mech. **14**(4), 529–551 (1962). https://doi.org/10.1017/S0022112062001421
104. P. O'Neill, J. Soria, D. Honnery, Exp. Fluids **36**(3), 473–483 (2004). https://doi.org/10.1007/s00348-003-0751-5
105. A.A. Putnam, J. Appl. Mech. Trans. ASME **30**(3), 476–477 (1960). https://doi.org/10.1115/1.3636593
106. H. Sato, F. Sakao, J. Fluid Mech. **20**(2), 337–352 (1964). https://doi.org/10.1017/S0022112064001264
107. T. Peacock, E. Bradley, J. Hertzberg, Y.C. Lee, Exp. Fluids **37**(1), 22–28 (2004). https://doi.org/10.1007/s00348-004-0780-8
108. A. Michalke, J. Fluid Mech. **19**(4), 543–556 (1964). https://doi.org/10.1017/S0022112064000908
109. A. Michalke, R. Wille, Proceedings of 11th International Congress on Applied Mechanics (1965)
110. Y. Ni, M.J. Lynch, M. Modic, R.D. Whalley, J.L. Walsh, J. Phys. D. Appl. Phys. **49**(35), 355203 (2016). https://doi.org/10.1088/0022-3727/49/35/355203
111. M.P. Hallberg, P.J. Srykowski, J. Fluid Mech. **569**, 493–507 (2006). https://doi.org/10.1017/S0022112006002357
112. T. Darny, J.M. Pouvesle, J. Fontane, L. Joly, S. Dozias, E. Robert, Plasma Sources Sci. Technol. **26**, 10 (2017). https://doi.org/10.1088/1361-6595/aa8877
113. C.C.W. Verlackt, W. Van Boxem, A. Bogaerts, Phys. Chem. Chem. Phys. **20**(10), 6845–6859 (2018). https://doi.org/10.1039/c7cp07593f
114. Y. Gorbanev, D. O'Connell, V. Chechik, Chem. Eur. J. **22**(10), 3496–3505 (2016). https://doi.org/10.1002/chem.201503771
115. Y. Gorbanev, C.C.W. Verlackt, S. Tinck, E. Tuenter, K. Foubert, P. Cos, A. Bogaerts, Phys. Chem. Chem. Phys. **20**(4), 2797–2808 (2018). https://doi.org/10.1039/c7cp07616a
116. K. Ostrikov, X. Yan, Z. Meng, J. Ouyang, Y. Qiao, J. Li, M. Jia, F. Yuan, J. Phys. D. Appl. Phys. **51**, 8 (2018). https://doi.org/10.1088/1361-6463/aaa867
117. B. Ghimire, J. Sornsakdanuphap, Y.J. Hong, H.S. Uhm, K.D. Weltmann, E.H. Choi, Phys. Plasmas **24**, 7 (2017). https://doi.org/10.1063/1.4989735
118. R. Zhou, R. Zhou, K. Prasad, Z. Fang, R. Speight, K. Bazaka, K. Ostrikov, Green Chem. **20**(23), 5276–5284 (2018). https://doi.org/10.1039/c8gc02800a
119. M. Xu, Y. Li, IEEE Trans. Plasma Sci. **47**(11), 4827–4832 (2019). https://doi.org/10.1109/TPS.2019.2928590
120. X. Zou, M. Xu, S. Pan, L. Gan, S. Zhang, H. Chen, D. Liu, X. Lu, K.K. Ostrikov, A.C.S. Biomater, Sci. Eng. **5**(3), 1611–1622 (2019). https://doi.org/10.1021/acsbiomaterials.9b00125
121. A. Bisag, P. Isabelli, R. Laurita, C. Bucci, F. Capelli, G. Dirani, M. Gherardi, G. Laghi, A. Paglianti, V. Sambri, V. Colombo, Plasma Process. Polym. (2020). https://doi.org/10.1002/ppap.202000154
122. E.V. Sysolyatina, A.Y. Lavrikova, R.A. Loleyt, E.V. Vasilieva, M.A. Abdulkadieva, S.A. Ermolaeva, A.V. Sofronov, Plasma Process. Polym. (2020). https://doi.org/10.1002/ppap.202000058
123. C. Freyssenet, S. Karlen, Appl. Biosaf. **24**(1), 10–19 (2019). https://doi.org/10.1177/1535676018818559
124. Y. Jiang, K. Sokorai, G. Pyrgiotakis, P. Demokritou, X. Li, S. Mukhopadhyay, T. Jin, X. Fan, Int. J. Food Microbiol. **249**, 53–60 (2017). https://doi.org/10.1016/j.ijfoodmicro.2017.03.004
125. Y. Song, B.A. Annous, X. Fan, Food Control **117** (2020). https://doi.org/10.1016/j.foodcont.2020.107358

126. T.R. Brubaker, K. Ishikawa, H. Kondo, T. Tsutsumi, H. Hashizume, H. Tanaka, S.D. Knecht, S.G. Bilén, M. Hori, J. Phys. D. Appl. Phys. **52**, 7 (2019). https://doi.org/10.1088/1361-6463/aaf460
127. D.T. Elg, I.W. Yang, D.B. Graves, J. Phys. D. Appl. Phys. **50**, 47 (2017). https://doi.org/10.1088/1361-6463/aa8f8c
128. M.M. Hefny, C. Pattyn, P. Lukes, J. Benedikt, J. Phys. D. Appl. Phys. **49**(40), 404002 (2016). https://doi.org/10.1088/0022-3727/49/40/404002
129. J.S. Oh, E.J. Szili, K. Ogawa, R.D. Short, M. Ito, H. Furuta, A. Hatta, Jpn. J. Appl. Phys. **57**, 1 (2018). https://doi.org/10.7567/JJAP.57.0102B9
130. W.P. Menashi, US Pat. 3,383,163, (1968)
131. M. Laroussi, G.S. Sayler, B.B. Glascock, B. McCurdy, M.E. Pearce, N.G. Bright, C.M. Malott, IEEE Trans. Plasma Sci. **27**(1), 34–35 (1999). https://doi.org/10.1109/27.763016
132. M. Laroussi, X. Lu, M. Keidar, J. Appl. Phys. **122**, 2 (2017). https://doi.org/10.1063/1.4993710
133. J. Golda, J. Held, B. Redeker, M. Konkowski, P. Beijer, A. Sobota, G. Kroesen, N.S.J. Braithwaite, S. Reuter, M.M. Turner, T. Gans, D. O'Connell, V. Schulz-Von Der Gathen, J. Phys. D. Appl. Phys. **49**, 8 (2016). https://doi.org/10.1088/0022-3727/49/8/084003
134. Gorbanev, Golda, Gathen, Bogaerts, Plasma **2**(3), 316–327 (2019). https://doi.org/10.3390/plasma2030023
135. D. Yan, J.H. Sherman, M. Keidar, 8(9) 15977–15995 (2016) . https://doi.org/10.18632/oncotarget.13304
136. J.H. Kim, M.A. Lee, G.J. Han, B.H. Cho, Acta Odontol. Scand. **72**(1), 1–12 (2014). https://doi.org/10.3109/00016357.2013.795660
137. S. Wu, Y. Cao, X. Lu, IEEE Trans. Plasma Sci. **44**(2), 134–151 (2016). https://doi.org/10.1109/TPS.2015.2506658
138. M. Laroussi, X. Lu, Appl. Phys. Lett. **87**, 11 (2005). https://doi.org/10.1063/1.2045549
139. M.G. Kong, G. Kroesen, G. Morfill, T. Nosenko, T. Shimizu, J. Van Dijk, J.L. Zimmermann, New J. Phys. **11** (2009). https://doi.org/10.1088/1367-2630/11/11/115012
140. F.C. Fang, Nat. Rev. Microbiol. **2**(10), 820–832 (2004). https://doi.org/10.1038/nrmicro1004
141. A.F.A. Fadhil, K. Fuliful, M.K. Khalaf, H.K. Oudah, J. Theor. Appl. Phys. **12**(1), 45–51 (2018). https://doi.org/10.1007/s40094-018-0279-y
142. Z. MacHala, L. Chldekov, M. Pelach, J. Phys. D. Appl. Phys. **43**, 22 (2010). https://doi.org/10.1088/0022-3727/43/22/222001
143. X. Lu, T. Ye, Y. Cao, Z. Sun, Q. Xiong, Z. Tang, Z. Xiong, J. Hu, Z. Jiang, Y. Pan, J. Appl. Phys. **104**, 5 (2008). https://doi.org/10.1063/1.2977674
144. J.W. Lackmann, S. Schneider, E. Edengeiser, F. Jarzina, S. Brinckmann, E. Steinborn, M. Havenith, J. Benedikt, J.E. Bandow, J.R. Soc, Interface **10**, 89 (2013). https://doi.org/10.1098/rsif.2013.0591
145. M.Y. Alkawareek, Q.T. Algwari, G. Laverty, S.P. Gorman, W.G. Graham, D. O'Connell, B.F. Gilmore, PLoS One **7**(8), 13–15 (2012). https://doi.org/10.1371/journal.pone.0044289
146. B. Kim, H. Yun, S. Jung, Y. Jung, H. Jung, W. Choe, C. Jo, Food Microbiol. **28**(1), 9–13 (2011). https://doi.org/10.1016/j.fm.2010.07.022
147. P.B. Flynn, S. Higginbotham, N.H. Alshraiedeh, S.P. Gorman, W.G. Graham, B.F. Gilmore, Int. J. Antimicrob. Agents **46**(1), 101–107 (2015). https://doi.org/10.1016/j.ijantimicag.2015.02.026
148. H.A. Aboubakr, P. Williams, U. Gangal, M.M. Youssef, S.A.A. El-sohaimy, P.J. Bruggeman, **81**(11), 3612–3622 (2015). https://doi.org/10.1128/AEM.00054-15
149. Z. Xu, J. Shen, C. Cheng, S. Hu, Y. Lan, P.K. Chu, J. Phys. D. Appl. Phys. **50**, 10 (2017). https://doi.org/10.1088/1361-6463/aa593f
150. Z. Machala, B. Tarabová, D. Sersenová, M. Janda, K. Hensel, J. Phys. D. Appl. Phys. **52**, 3 (2019). https://doi.org/10.1088/1361-6463/aae807
151. J.L. Brisset, E. Hnatiuc, Plasma Chem. Plasma Process. **32**(4), 655–674 (2012). https://doi.org/10.1007/s11090-012-9384-x
152. F. Girard, V. Badets, S. Blanc, K. Gazeli, L. Marlin, L. Authier, P. Svarnas, N. Sojic, F. Clément, S. Arbault, RSC Adv. **6**(82), 78457–78467 (2016). https://doi.org/10.1039/c6ra12791f
153. E. Dolezalova, P. Lukes, Bioelectrochemistry **103**, 7–14 (2015). https://doi.org/10.1016/j.bioelechem.2014.08.018
154. U.K. Ercan, B. Sen, A.D. Brooks, S.G. Joshi, J. Appl. Microbiol. **125**(2), 383–397 (2018). https://doi.org/10.1111/jam.13777
155. P.J. Bruggeman, M.J. Kushner, B.R. Locke, J.G.E. Gardeniers, W.G. Graham, D.B. Graves, R.C.H.M. Hofman-Caris, D. Maric, J.P. Reid, E. Ceriani, D. Fernandez Rivas, J.E. Foster, S.C. Garrick, Y. Gorbanev, S. Hamaguchi, F. Iza, H. Jablonowski, E. Klimova, J. Kolb, F. Krcma, P. Lukes, Z. MacHala, I. Marinov, D. Mariotti, S. Mededovic Thagard, D. Minakata, E.C. Neyts, J. Pawlat, Z.L. Petrovic, R. Pflieger, S. Reuter, D.C. Schram, S. Schröter, M. Shiraiwa, B. Tarabová, P.A. Tsai, J.R.R. Verlet, T. Von Woedtke, K.R. Wilson, K. Yasui, G. Zvereva, Plasma Sources Sci. Technol. 25(5) (2016). https://doi.org/10.1088/0963-0252/25/5/053002
156. H. Hülsheger, J. Potel, E.G. Niemann, Radiat. Environ. Biophys. **22**(2), 149–162 (1983). https://doi.org/10.1007/BF01338893
157. P. Estifaee, X. Su, S.K. Yannam, S. Rogers, S.M. Thagard, Sci. Rep. **9**(1), 1–12 (2019). https://doi.org/10.1038/s41598-019-38838-7
158. M. Dezest, A.L. Bulteau, D. Quinton, L. Chavatte, M. Le Bechec, J.P. Cambus, S. Arbault, A. Nègre-Salvayre, F. Cleâment, S. Cousty, PLoS One **12**(3), 1–18 (2017). https://doi.org/10.1371/journal.pone.0173618
159. M.A. Sharkey, A. Chebbi, K.A. McDonnell, C. Staunton, D.P. Dowling, Biointerphases **10**(2), 029507 (2015). https://doi.org/10.1116/1.4916928
160. S.A. Ermolaeva, A.F. Varfolomeev, M.Y. Chernukha, D.S. Yurov, M.M. Vasiliev, A.A. Kaminskaya, M.M. Moisenovich, J.M. Romanova, A.N. Murashev, I.I. Selezneva, T. Shimizu, E.V. Sysolyatina, I.A. Shaginyan, O.F. Petrov, E.I. Mayevsky, V.E. Fortov, G.E. Morfill, B.S. Naroditsky, A.L. Gintsburg, J. Med. Microbiol. **60**(1), 75–83 (2011). https://doi.org/10.1099/jmm.0.020263-0
161. N. Ulbin-Figlewicz, A. Jarmoluk, K. Marycz, Ann. Microbiol. **65**(3), 1537–1546 (2015). https://doi.org/10.1007/s13213-014-0992-y

162. X. Liao, D. Liu, Q. Xiang, J. Ahn, S. Chen, X. Ye, T. Ding, Food Control **75**, 83–91 (2017). https://doi.org/10.1016/j.foodcont.2016.12.021
163. A. Mai-Prochnow, M. Clauson, J. Hong, A.B. Murphy, Sci. Rep. **6**(November), 1–11 (2016). https://doi.org/10.1038/srep38610
164. M. Modic, J. Kovač, J.R. Nicholls, Š. Kos, G. Serša, U. Cvelbar, J.L. Walsh, Appl. Surf. Sci. **487**(May), 1176–1188 (2019). https://doi.org/10.1016/j.apsusc.2019.05.153
165. M. Modic, N.P. McLeod, J.M. Sutton, J.L. Walsh, Int. J. Antimicrob. Agents **49**(3), 375–378 (2017). https://doi.org/10.1016/j.ijantimicag.2016.11.022
166. Z. Xiong, T. Du, X. Lu, Y. Cao, Y. Pan, Appl. Phys. Lett. **98**(22), 3–6 (2011). https://doi.org/10.1063/1.3597622
167. W.M. Dunne, Clin. Microbiol. Rev. **15**(2), 155–166 (2002). https://doi.org/10.1128/CMR.15.2.155-166.2002
168. W. Van Gaens, S. Iseni, A. Schmidt-Bleker, K.D. Weltmann, S. Reuter, A. Bogaerts, New J. Phys. **17** (2015). https://doi.org/10.1088/1367-2630/17/3/033003
169. D.X. Liu, Z.C. Liu, C. Chen, A.J. Yang, D. Li, M.Z. Rong, H.L. Chen, M.G. Kong, Sci. Rep. **6** (2016). https://doi.org/10.1038/srep23737
170. G.C. Gurtner, S. Werner, Y. Barrandon, M.T. Longaker, Nature **453**(7193), 314–321 (2008). https://doi.org/10.1038/nature07039
171. T. Velnar, T. Bailey, V. Smrkolj, J. Int. Med. Res. **37**(5), 1528–1542 (2009). https://doi.org/10.1177/147323000903700531
172. P. Brun, S. Pathak, I. Castagliuolo, G. Palù, P. Brun, M. Zuin, R. Cavazzana, E. Martines, PLoS One **9**(8), 1–9 (2014). https://doi.org/10.1371/journal.pone.0104397
173. J. Liu, G. Xu, X. Shi, G. Zhang, Sci. Rep. (May) 1–12 (2017). https://doi.org/10.1038/s41598-017-12043-w
174. X. Shi, J. Cai, G. Xu, H. Ren, S. Chen, Z. Chang, J. Liu, C. Huang, G. Zhang, X. Wu, Plasma Sci. Technol. **18**(4), 353–359 (2016). https://doi.org/10.1088/1009-0630/18/4/04
175. A. Schmidt, S. Dietrich, A. Steuer, K.D. Weltmann, T. Von Woedtke, K. Masur, K. Wende, J. Biol. Chem. **290**(11), 6731–6750 (2015). https://doi.org/10.1074/jbc.M114.603555
176. S. Blackert, B. Haertel, K. Wende, T. von Woedtke, U. Lindequist, J. Dermatol. Sci. **70**(3), 173–181 (2013). https://doi.org/10.1016/j.jdermsci.2013.01.012
177. K. Wende, P. Williams, J. Dalluge, W. Van Gaens, H. Aboubakr, J. Bischof, T. von Woedtke, S.M. Goyal, K.-D. Weltmann, A. Bogaerts, K. Masur, P.J. Bruggeman, Biointerphases **10**(2), 029518 (2015). https://doi.org/10.1116/1.4919710
178. S. Kubinova, K. Zaviskova, L. Uherkova, V. Zablotskii, O. Churpita, O. Lunov, A. Dejneka, Sci. Rep. **7**(February), 1–11 (2017). https://doi.org/10.1038/srep45183
179. M. Chatraie, G. Torkaman, M. Khani, H. Salehi, B. Shokri, Sci. Rep. **8**(1), 1–11 (2018). https://doi.org/10.1038/s41598-018-24049-z
180. A.V. Nastuta, I. Topala, C. Grigoras, V. Pohoata, G. Popa, J. Phys. D. Appl. Phys. **44**, 10 (2011). https://doi.org/10.1088/0022-3727/44/10/105204
181. S. Arndt, P. Unger, E. Wacker, T. Shimizu, J. Heinlin, Y.F. Li, H.M. Thomas, G.E. Morfill, J.L. Zimmermann, A.K. Bosserhoff, S. Karrer, PLoS One **8**(11), 1–9 (2013). https://doi.org/10.1371/journal.pone.0079325
182. J.H. Choi, Y.S. Song, K. Song, H.J. Lee, J.W. Hong, G.C. Kim, Sci. Rep. **7**(1), 1–11 (2017). https://doi.org/10.1038/s41598-017-06661-7
183. Y. Nomura, T. Takamatsu, H. Kawano, H. Miyahara, A. Okino, M. Yoshida, T. Azuma, J. Surg. Res. **219**, 302–309 (2017). https://doi.org/10.1016/j.jss.2017.06.055
184. C. Ulrich, F. Kluschke, A. Patzelt, S. Vandersee, V.A. Czaika, H. Richter, A. Bob, J. Von Hutten, C. Painsi, R. Hügel, A. Kramer, O. Assadian, J. Lademann, B. Lange-Asschenfeldt, J. Wound Care **24**(5), 196–203 (2015). https://doi.org/10.12968/jowc.2015.24.5.196
185. H.R. Metelmann, T.T. Vu, H.T. Do, T.N.B. Le, T.H.A. Hoang, T.T.T. Phi, T.M.L. Luong, V.T. Doan, T.T.H. Nguyen, T.H.M. Nguyen, T.L. Nguyen, D.Q. Le, T.K.X. Le, T. von Woedtke, R. Bussiahn, K.D. Weltmann, R. Khalili, F. Podmelle, Clin. Plasma Med. **1**(1), 30–35 (2013). https://doi.org/10.1016/j.cpme.2012.12.001
186. O. Lademann, A. Kramer, H. Richter, A. Patzelt, M.C. Meinke, V. Czaika, K.D. Weltmann, B. Hartmann, S. Koch, Skin Pharmacol. Physiol. **24**(5), 284–288 (2011). https://doi.org/10.1159/000329913
187. S. Vandersee, H. Richter, J. Lademann, M. Beyer, A. Kramer, F. Knorr, B. Lange-Asschenfeldt, Laser Phys. Lett. **11**, 11 (2014). https://doi.org/10.1088/1612-2011/11/11/115701
188. F. Brehmer, H.A. Haenssle, G. Daeschlein, R. Ahmed, S. Pfeiffer, A. Görlitz, D. Simon, M.P. Schön, D. Wandke, S. Emmert, J. Eur. Acad. Dermatol. Venereol. **29**(1), 148–155 (2015). https://doi.org/10.1111/jdv.12490
189. A. Chuangsuwanich, T. Assadamongkol, D. Boonyawan, Int. J. Low. Extrem. Wounds **15**(4), 313–319 (2016). https://doi.org/10.1177/1534734616665046
190. S. Hartwig, C. Doll, J.O. Voss, M. Hertel, S. Preissner, J.D. Raguse, J. Oral Maxillofac. Surg. **75**(2), 429–435 (2017). https://doi.org/10.1016/j.joms.2016.08.011
191. J. Heinlin, J.L. Zimmermann, F. Zeman, W. Bunk, G. Isbary, M. Landthaler, T. Maisch, R. Monetti, G. Morfill, T. Shimizu, J. Steinbauer, W. Stolz, S. Karrer, Wound Repair Regen. **21**(6), 800–807 (2013). https://doi.org/10.1111/wrr.12078
192. G. Isbary, G. Morfill, H.U. Schmidt, M. Georgi, K. Ramrath, J. Heinlin, S. Karrer, M. Landthaler, T. Shimizu, B. Steffes, W. Bunk, R. Monetti, J.L. Zimmermann, R. Pompl, W. Stolz, Br. J. Dermatol. **163**(1), 78–82 (2010). https://doi.org/10.1111/j.1365-2133.2010.09744.x
193. G. Isbary, J. Heinlin, T. Shimizu, J.L. Zimmermann, G. Morfill, H.U. Schmidt, R. Monetti, B. Steffes, W. Bunk, Y. Li, T. Klaempfl, S. Karrer, M. Landthaler, W. Stolz, Br. J. Dermatol. **167**(2), 404–410 (2012). https://doi.org/10.1111/j.1365-2133.2012.10923.x
194. G. Isbary, T. Shimizu, J.L. Zimmermann, H.M. Thomas, G.E. Morfill, W. Stolz, New Microbes New Infect. **1**(3), 41–43 (2013). https://doi.org/10.1002/2052-2975.19
195. M. Klebes, C. Ulrich, F. Kluschke, A. Patzelt, S. Vandersee, H. Richter, A. Bob, J. von Hutten, J.T. Krediet,

A. Kramer, J. Lademann, B. Lange-Asschenfeld, J. Biophoton. **8**(5), 382–391 (2015). https://doi.org/10.1002/jbio.201400007
196. S. Arndt, Clin. Plasma Med. **9**(November 2017), 24–33 (2018). https://doi.org/10.1016/j.cpme.2018.01.002
197. E.J. Szili, S.H. Hong, J.S. Oh, N. Gaur, R.D. Short, Trends Biotechnol. **36**(6), 594–602 (2018). https://doi.org/10.1016/j.tibtech.2017.07.012
198. A. Schmidt, T. von Woedtke, J. Stenzel, T. Lindner, S. Polei, B. Vollmar, S. Bekeschus, Int. J. Mol. Sci. **18**(4), 1–19 (2017). https://doi.org/10.3390/ijms18040868
199. A. Mesbah, D.B. Graves, J. Phys. D. Appl. Phys. **52**, 30 (2019). https://doi.org/10.1088/1361-6463/ab1f3f
200. K. Reineke, K. Langer, C. Hertwig, J. Ehlbeck, O. Schlüter, Innov. Food Sci. Emerg. Technol. **30**, 112–118 (2015). https://doi.org/10.1016/j.ifset.2015.03.019
201. T. Takamatsu, K. Uehara, Y. Sasaki, M. Hidekazu, Y. Matsumura, A. Iwasawa, N. Ito, M. Kohno, T. Azuma, A. Okino, PLoS One **10**(7), 1–9 (2015). https://doi.org/10.1371/journal.pone.0132381
202. P. Lukes, E. Dolezalova, I. Sisrova, M. Clupek, Plasma Sources Sci. Technol. **23**, 1 (2014). https://doi.org/10.1088/0963-0252/23/1/015019
203. M. Baier, J. Foerster, U. Schnabel, D. Knorr, J. Ehlbeck, W.B. Herppich, O. Schlüter, Postharvest Biol. Technol. **84**, 81–87 (2013). https://doi.org/10.1016/j.postharvbio.2013.03.022
204. Q. Xiang, C. Kang, D. Zhao, L. Niu, X. Liu, Y. Bai, Food Control **99**(136), 28–33 (2019). https://doi.org/10.1016/j.foodcont.2018.12.019
205. L. Chandana, C.J. Sangeetha, T. Shashidhar, C. Subrahmanyam, Sci. Total Environ. **640–641**, 493–500 (2018). https://doi.org/10.1016/j.scitotenv.2018.05.342
206. Z. Ke, Q. Zhang, Q. Huang, ACS Omega **4**(5), 8365–8372 (2019). https://doi.org/10.1021/acsomega.9b00160
207. G. Asadollahfardi, M. Khandan, S.H. Aria, Contrib. Plasma Phys. (August 2018) 1–7 (2019) . https://doi.org/10.1002/ctpp.201800106
208. T. Royintarat, P. Seesuriyachan, D. Boonyawan, E.H. Choi, W. Wattanutchariya, Curr. Appl. Phys. **19**(9), 1006–1014 (2019). https://doi.org/10.1016/j.cap.2019.05.020
209. S.G. Bilén, S.D. Knec, G.S. Kiriman, 1–11 (2020). https://doi.org/10.1038/s41598-020-59652-6
210. K. Lotfy, AIP Adv. **10**, 1 (2020). https://doi.org/10.1063/1.5099923
211. S. Winter, A. Meyer-Lindenberg, G. Wolf, S. Reese, M.C. Nolff, J. Microbiol. Methods **169**, 2020 (2019). https://doi.org/10.1016/j.mimet.2019.105728
212. K. Itooka, K. Takahashi, Y. Kimata, S. Izawa 2279–88 (2018)
213. J. Shen, H. Zhang, Z. Xu, Z. Zhang, C. Cheng, G. Ni, Y. Lan, Chem. Eng. J. **362**(January), 402–412 (2019). https://doi.org/10.1016/j.cej.2019.01.018
214. A. Chiodi, T. Mayumi, C. Nishime, K. Georgiev, G. De Morais, G. Lima, A. Vidal, L. Gontijo, J. Nóbrega, M. Marchesotti, D. Carvalho, R. Yzumi, Clin. Plasma Med. **7–8**(January), 9–15 (2017). https://doi.org/10.1016/j.cpme.2017.06.002
215. D. Li, G. Li, J. Li, Z.-Q. Liu, X. Zhang, Y. Zhang, H.-P. Li, IEEE Trans. Plasma Sci. **47**(1), 1–13 (2019). https://doi.org/10.1109/tps.2019.2928320
216. Z. Shahbazi Rad, F. Abbasi Davani, G. Etaati, Australas, Phys. Eng. Sci. Med. **41**(4), 905–917 (2018). https://doi.org/10.1007/s13246-018-0686-z
217. G.M. Xu, X.M. Shi, J.F. Cai, S. Le Chen, P. Li, C.W. Yao, Z.S. Chang, G.J. Zhang, Wound Repair Regen. **23**(6), 878–884 (2015). https://doi.org/10.1111/wrr.12364
218. S. Darmawati, A. Rohmani, L.H. Nurani, M.E. Prastiyanto, S.S. Dewi, N. Salsabila, E.S. Wahyuningtyas, F. Murdiya, I.M. Sikumbang, R.N. Rohmah, Y.A. Fatimah, A. Widiyanto, T. Ishijima, J. Sugama, T. Nakatani, N. Nasruddin, Clin. Plasma Med. **14**(18), 100085 (2019). https://doi.org/10.1016/j.cpme.2019.100085
219. Y. Nasruddin, K. Nakajima, H.S.E. Mukai, M. Rahayu, T. Nur, H. Ishijima, Y. Enomoto, J. Uesugi, T. Sugama, Nakatani, Clin. Plasma Med. **2**(1), 28–35 (2014). https://doi.org/10.1016/j.cpme.2014.01.001
220. Y.W. Hung, L.T. Lee, Y.C. Peng, C.T. Chang, Y.K. Wong, K.C. Tung, J. Chinese Med. Assoc. **79**(6), 320–328 (2016). https://doi.org/10.1016/j.jcma.2015.06.024
221. Z.H. Lin, K.Y. Cheng, Y.P. Cheng, C.Y.T. Tschang, H.Y. Chiu, N.L. Yeh, K.C. Liao, B.R. Gu, J.S. Wu, Plasma Med. **7**(3), 227–244 (2017). https://doi.org/10.1615/PlasmaMed.2017020386
222. S. Salehi, A. Shokri, M.R. Khani, M. Bigdeli, B. Shokri, Biointerphases **10**(2), 029504 (2015). https://doi.org/10.1116/1.4914377
223. K.Y. Cheng, Z.H. Lin, Y.P. Cheng, H.Y. Chiu, N.L. Yeh, T.K. Wu, J.S. Wu, Sci. Rep. **8**(1), 1–15 (2018). https://doi.org/10.1038/s41598-018-30597-1
224. O. Lunov, V. Zablotskii, O. Churpita, A. Jäger, L. Polívka, E. Syková, N. Terebova, A. Kulikov, Š. Kubinová, A. Dejneka, RSC Adv. **6**(30), 25286–25292 (2016). https://doi.org/10.1039/c6ra02368a
225. O. Lunov, O. Churpita, V. Zablotskii, I.G. Deyneka, I.K. Meshkovskii, A. Jäger, E. Syková, Kubinová, A. Dejneka, Appl. Phys. Lett. **106**(5) (2015). https://doi.org/10.1063/1.4907624
226. M. Kurosawa, T. Takamatsu, S. Ota, A. Okino, J. Surg. Res. **234**, 334–342 (2018). https://doi.org/10.1016/j.jss.2018.09.068
227. E. Martines, P. Brun, R. Cavazzana, L. Cordaro, M. Zuin, T. Martinello, C. Gomiero, A. Perazzi, L. Melotti, L. Maccatrozzo, M. Patruno, I. Iacopetti, Clin. Plasma Med. **17–18**(July 2019), 100095 (2020). https://doi.org/10.1016/j.cpme.2020.100095
228. T. Kisch, S. Schleusser, A. Helmke, K.L. Mauss, E.T. Wenzel, B. Hasemann, P. Mailaender, R. Kraemer, Microvasc. Res. **106**, 8–13 (2016). https://doi.org/10.1016/j.mvr.2016.02.008
229. M. Weiss, J. Barz, M. Ackermann, R. Utz, A. Ghoul, K.D. Weltmann, M.B. Stope, D. Wallwiener, K. Schenke-Layland, C. Oehr, S. Brucker, P. Loskill, A.C.S. Appl, Mater. Interfaces **11**(22), 19841–19853 (2019). https://doi.org/10.1021/acsami.9b04803